NACA

RESEARCH MEMORANDUM

EXPERIMENTAL INVESTIGATION OF THE STATIC AERODYNAMIC AND

DYNAMIC DAMPING-IN-ROLL CHARACTERISTICS OF AN 8-CM

AIRCRAFT ROCKET WITH SOLID AND SLOTTED FINS

By Robert S. Chubb

Ames Aeronautical Laboratory
Moffett Field, Calif.

ssification cancelled (or changed to ...Unclassified...)

By authority of Nasa Tech. Pub Announcement #128
(OFFICER AUTHORIZED TO CHANGE)

28 July 58

By ....
NAME AND

GRADE OF OFFICER MAKING CHANGE)

20 April 61
DATE

NATIONAL ADVISORY COMMITTEE
FOR AERONAUTICS
WASHINGTON
June 2, 1952

TABLE OF CONTENTS

TABLE OF CONTENTS - Continued
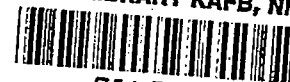
NATIONAL ADVISORY COMMITTEE FOR AERONAUTICS

RESEARCH MEMORANDUM

EXPERIMENTAL INVESTIGATION OF THE STATIC AERODYNAMIC AND

DYNAMIC DAMPING-IN-ROLL CHARACTERISTICS OF AN 8-CM

AIRCRAFT ROCKET WITH SOLID AND SLOTTED FINS

By Robert S. Chubb

SUMMARY

The static aerodynamic and dynamic damping-in-roll characteristics
of an 8-cm aircraft rocket having cruciform fins of trapezoidal plan
form were determined experimentally at various Mach numbers ranging
from 0.6 to 1.9. The stabilizing fins of the rocket are of unusual
design in that two holes are cut through each fin panel; the effects of
these holes or slots were investigated by testing with both solid and
slotted fins.

The most distinctive effect due to the slots in the stabilizing
fins was noted in the static rolling-moment characteristics of the
rocket at supersonic speeds as determined from tests at a Mach number
of 1.7. The solid-fin configuration exhibited very erratic rolling-
moment characteristics as a function of angle of attack, particularly at
large angles, at various roll positions; whereas the slotted-fin con-
figuration exhibited little or no rolling moment at any roll position.
It was concluded, therefore, that the slots tend to suppress any adverse
rolling tendencies induced on the fins by the long forebody. The static
normal-force and pitching-moment characteristics were unchanged with
roll position for both the solid- and slotted-fin configurations; how-
ever, the normal-force and pitching-moment coefficients of the rocket
with slotted fins were less than those for the solid-fin configuration
by an amount approximately commensurate with the reduction in area due
to the slots (M = 1.7). The rocket also exhibited statically stable
characteristics at subsonic speeds as determined at a representative Mach
number of 0.7. Axial-force coefficients of the slotted-fin arrangement
at 0° angle of attack were increased about 15 percent over those for the
solid-fin arrangement at Mach numbers ranging from 0.6 to 0.92 and 1.2
to 1.7.

The experimental damping-in-roll coefficients of the solid-fin con-
figuration at 0° angle of attack (M = 1.5, 1.7, 1.9) were found to agree
quite closely with those predicted by linear theory for thin rectangular
wings. The damping-in-roll coefficients of the slotted fins were 15
to 25 percent less than those predicted by linear theory for solid fins.
The slotted-fin damping-in-roll coefficients were relatively constant
with angle of attack, whereas those of the solid fins varied approximately
20 percent over an angle range from -1° to 5°.

INTRODUCTION

At the request of the Bureau of Ordnance of the Department of the
Navy, an investigation of the aerodynamic properties of an 8-cm aircraft
rocket was undertaken in the Ames 6- by 6-foot supersonic wind tunnel.
The rocket consists of an ogival nose, cylindrical body, and stabilizing
fins of trapezoidal plan form and cruciform arrangement. The stabiliz-
ing fins are unusual in that two large elongated holes or slots have
been cut through each panel of the fins. To provide a basis of compari-
son for determining the effects of these slots, the investigation
included a solid-fin configuration as well as the slotted-fin configu-
ration. Also included were two nose or head types: (1) a standard high-
explosive head, and (2) a high-explosive antitank head.

The rocket is spin stabilized during the acceleration period of its
flight by canting the exhaust nozzles with respect to the longitudinal
body axis. After the propellant charge has been expended, there is no
longer an applied torque and the rolling angular velocity is reduced by
the aerodynamic damping with a consequent adverse influence on the
accuracy of the rocket.

The investigation was divided into two parts: (1) determination of
the static aerodynamic characteristics, and (2) determination of the
dynamic damping-in-roll characteristics. The results of both parts of
the investigation are presented herein.

SYMBOLS

A   rolling moment due to asymmetry of the model and/or tunnel
        air stream, pound-feet

A_b cross-sectional area of the body at the base, 0.0554 square foot

AR   aspect ratio, 1.635

b   span in the plane of the fins, 0.659 foot

d   diameter of the body, 0.266 foot

F_p rolling moment due to friction per unit rolling angular velocity, pound-foot seconds per radian

H   total pressure, pounds per square foot

I_x mass moment of inertia about the longitudinal body axis, 0.01 pound-foot seconds squared

k $\dfrac{L_p + F_p}{I_x}$

L_p rolling moment due to aerodynamic damping per unit rolling angular velocity, pound-foot seconds per radian

M   Mach number

p   rolling angular velocity, radians per second

p_a autorotational rolling angular velocity, radians per second

p_o initial rolling angular velocity (p when t = 0), radians per second

q   free-stream dynamic pressure, pounds per square foot

R   Reynolds number based on the body diameter

S   area of four solid fins including the area enclosed by the body, 0.521 square foot

t   time, seconds

V   free-stream velocity, feet per second

α angle of attack, degrees

β $\sqrt{M^2 - 1}$

φ angle of roll, degrees

C_N normal-force coefficient $\left(\dfrac{\text{normal force}}{qA_b} \right)$

C_X axial-force coefficient $\left(\dfrac{\text{axial force}}{qA_b}\right)$

C_m pitching-moment coefficient about the center of gravity $\left(\dfrac{\text{pitching moment}}{qdA_b}\right)$

C_l rolling-moment coefficient about the longitudinal body axis $\left(\dfrac{\text{rolling moment}}{qbA_b}\right)$

C_{N_α} $\dfrac{\partial C_N}{\partial \alpha}$

$C_{m_{C_N}}$ $\dfrac{\partial C_m}{\partial C_N}$

C_{l_p} damping-in-roll coefficient about the longitudinal body axis $\left[\dfrac{L_p}{\left(\dfrac{b}{2V}\right)qbS}\right]$

APPARATUS AND MODEL

Tunnel

The present investigation was conducted in the Ames 6- by 6-foot supersonic wind tunnel. This tunnel is of the single-return closed-circuit type in which the stagnation pressure can be regulated to give a constant test Reynolds number. The test-section Mach number can be varied continuously from 0.6 to 0.92 and 1.2 to 1.9. Further details concerning the tunnel are presented in reference 1.

Model

A photograph of the 8-cm aircraft rocket mounted in the Ames 6- by 6-foot supersonic wind tunnel is shown in figure 1. The model tested was a full-scale production rocket provided with interchangeable high-explosive (HE) and high-explosive antitank (HEAT) heads. Cruciform stabilizing fins of trapezoidal plan form were stamped from sheet steel

and spot welded to the removable cylindrical motor tube. The geometric characteristics of the 8-cm aircraft rocket and its component parts are shown in figure 2. The center of gravity was located 5.06 body diameters forward of the base; the mass moment of inertia of the rocket about the longitudinal body axis was determined experimentally as 0.01 pound-feet seconds squared ±3 percent. The same rocket was used for both static and dynamic tests.

Equipment

Static test system.- The static aerodynamic forces and moments on the model were measured by a 2-1/2-inch diameter, four component, strain-gage balance contained within the body of the model and mounted on a sting-type support. The 2-1/2-inch-diameter balance is described in reference 2. Reduction of the measured forces and moments to coefficient form is discussed in a later section. Static pressure at the model base was measured by means of a static pressure tube attached to the sting support. The ratio of the sting diameter to body diameter at the model base was 0.56.

Dynamic-roll test system.- For the dynamic-roll tests the rocket was mounted on the sting-type support with bearings so that the model was free to rotate about the longitudinal body axis. A motor-clutch mechanism was used to accelerate the model up to the desired initial rolling angular velocity; the damping in roll was obtained by disengaging the clutch and measuring the decay of the rolling velocity from time histories of the roll position. These time histories of the roll position were recorded on an oscillograph by means of a pulse signal transmitted through a brush-type contact each quarter revolution. A portion of a sample time history is shown in figure 3. Every fourth signal represents the same roll position and the distance between adjacent signals represents the time to roll a quarter revolution. The method of reducing the data obtained in this manner is discussed in a later section.

STATIC AERODYNAMIC CHARACTERISTICS

Range of Tests

Measurements were made of normal force, axial force, pitching moment, and rolling moment at nominal angles of attack from -4° to 18° for a Mach number of 1.7 and each of the following configurations and roll angles:

HE head, solid fins:	0°, 11.25°, 22.5°, 33.75°, 45°
HE head, slotted fins:	0°, 11.25°, 22.5°, 33.75°, 45°
HEAT head, solid fins:	0°
HEAT head, slotted fins:	0°

The same configurations were also tested at a Mach number of 0.7, but the roll angles were limited to 0°. The axial force was measured at Mach numbers from 0.6 to 0.92 and 1.2 to 1.7 at a nominal angle of attack of 0° and roll angle of 0°, for each of the above configurations. All of the static test data were obtained at a Reynolds number of 0.85×10^6 based on the body diameter.

Reduction of Data

The internal strain-gage balance used to measure the aerodynamic forces and moments on the model is oriented with respect to the model such that the balance readings give the normal force, axial force, rolling moment about the longitudinal body axis of the model, and pitching moment referred to an arbitrarily selected lateral axis. The balance was calibrated prior to the test by loading the balance statically at various longitudinal positions. To find the transfer factor necessary to translate the pitching moments about the balance lateral axis to any other axis, for instance one through the center of gravity, the model is loaded statically at that point, the center of gravity, and the transfer factor calculated from measurements of pitching moment and normal force. All forces and moments calculated from the test data have been reduced to coefficient form as defined in the section entitled "Symbols."

It should be noted that the axial-force coefficients presented are based on forebody forces only since the measured axial forces were adjusted to zero base drag by utilizing the measured difference between the model base pressure and the free-stream static pressure.

Corrections

Several corrections to the test data are necessary due to factors which affect the accuracy of the results. Each correction will be discussed individually to show not only those necessary, but also those considered negligible.

Deflection of support system.- The model support system and strain-gage balance deflect under load. Corrections to the angle of attack due to these deflections were calculated from calibrations obtained by loading the model statically prior to the test.

Stream variations.- Preliminary tests of the 8-cm rocket in the Ames 6- by 6-foot supersonic wind tunnel showed the effects of flow angularity of the stream on the model aerodynamic characteristics to be within the experimental accuracy (see section entitled "Precision") of the tests both for subsonic and supersonic speeds; hence, these corrections are considered negligible.

Small axial static pressure gradients exist in the 6- by 6-foot tunnel causing a longitudinal buoyant force on the model. Corrections for this buoyant force were calculated from the flow studies of reference 1.

Support interference.- It was shown in reference 3 that at supersonic speeds the effects of support interference were evinced solely as a change in base pressure for body-support systems of the present type. The adjustment of the measured axial forces to correspond to zero base drag, mentioned earlier, therefore obviates the necessity of any correction of the data for support interference. The effects of support interference at subsonic speeds are not known. However, it was assumed that the same adjustment precludes any corrections at these speeds also.

Tunnel-wall interference.- The flow of the air stream around the model was viewed by use of a schlieren apparatus. Compression waves emanating from the nose of the model at supersonic speeds were reflected from the tunnel walls and were observed to pass downstream of the base of the model; hence, no corrections were necessary at these speeds. Calculations for subsonic speeds showed that corrections to angle of attack, normal force, and pitching moment due to induced effects of the tunnel walls were within the accuracy of measurement of the corresponding characteristic; hence, no corrections were necessary at these speeds as well.

Blockage effects of the model.- Mounting the model in the air stream has an effect of blocking the test section or causing an increase in velocity along the length of the model at subsonic speeds. The effects of blockage of the test section have been calculated by the method of reference 4 for 0° angle of attack and assumed to apply for all angles of attack. The correction in Mach number varied from 0.2 percent increase at a Mach number of 0.6 to 1 percent increase at a Mach number of 0.92.

Precision

The precision of the static test data has been estimated from the known uncertainties involved in determining or measuring various quantities. These uncertainties arise from errors in reading pressures, recording strain-gage voltages and currents, hysteresis effects in

calibrating the balance, and measurement of angles. The following table lists the estimated uncertainty of the corresponding quantity:

Quantity	Subsonic	Supersonic
Mach number	0.01	0.01
Reynolds number	0.01×10^6	0.03×10^6
Normal-force coefficient	0.005	0.01
Axial-force coefficient	0.005	0.01
Pitching-moment coefficient	0.05	0.1
Rolling-moment coefficient	0.001	0.002
Angle of attack, degrees	0.05	0.05
Angle of roll, degrees	0.20	0.20

Results and Discussion

A primary consideration in the design of any rocket is the ability of the propellant charge to overcome the resisting aerodynamic forces during the initial accelerating period. To assist in predicting the accelerating and maximum speed characteristics of the 8-cm aircraft rocket, the variation of axial-force coefficient with Mach number at 0° angle of attack is presented in figure 4 for each of the following configurations: (a) solid fins, HE head; (b) solid fins, HEAT head; (c) slotted fins, HE head; (d) slotted fins, HEAT head. The average increase in axial-force coefficient due to slotted fins amounted to about 15 percent of the solid-fin values throughout the Mach number range; in general, the increase due to the HEAT head amounted to 5 to 10 percent of the HE head values at subsonic speeds and 30 to 35 percent at supersonic speeds.

Basic experimental data plots of the normal force, axial force, and pitching-moment characteristics of the 8-cm aircraft rocket at Mach numbers of 0.7 and 1.7 are presented in figures 5 and 6 for each of the configurations listed above. Although the rocket accelerates rapidly to supersonic velocity, the purpose of the data taken at M = 0.7 was to ascertain if there were any unfavorable stability characteristics at this intermediate speed. As seen in parts (a) of figures 5 and 6, the rocket is longitudinally (also directionally due to symmetry) stable for M = 0.7 within the angle-of-attack range tested with both solid and slotted fins, although there is a reduction in normal-force coefficient and pitching-moment coefficient due to the use of slotted fins.

At supersonic speed, a representative Mach number of 1.7 was selected for investigation of the static aerodynamic characteristics. Parts (b) of figures 5 and 6 show that the rocket exhibits stable restoring moments ($C_{m_{C_N}}$ negative) within the lower angle-of-attack range and

at the higher angles $C_{m_{C_N}}$ approaches zero. The effect of the slotted
fins follows generally the trend to be expected; at any given angle of
attack the normal-force and pitching-moment coefficients of the slotted-
fin configuration were reduced from solid-fin values by an amount approx-
imately commensurate with the reduction in area.

All the afore-mentioned data were taken with the cruciform fins in
the vertical and horizontal planes $(\varphi = 0^\circ)$. It was desired to deter-
mine as well the static aerodynamic characteristics of the rocket at
several intermediate roll angles. The normal-force, pitching-moment,
axial-force, and rolling-moment characteristics of the rocket at roll
angles of 0°, 11.25°, 22.5°, 33.75°, and 45° and a Mach number of 1.7
are presented in figures 7 and 8 for the solid- and slotted-fin configu-
rations, respectively. Normal-force, pitching-moment, and axial-force
coefficients are seen to be essentially unchanged with roll position;
however, the variation of rolling-moment coefficient with normal-force
coefficient appears to be influenced to a large degree by roll position,
especially at the higher normal-force coefficients.

The apparent scatter in the rolling-moment data is due primarily
to flexibility of the support system. In order to measure rolling
moments of the order of magnitude obtained in the present test, it was
necessary to utilize a roll gage of relatively light torsional rigidity.
As a consequence, the model experienced a small dynamic oscillation in
roll, the limits of which were assumed to be the limits of the apparent
scatter. The point midway between the limits of the oscillation was
assumed, therefore, to be a reasonably accurate estimate of the static
rolling moment.

In figure 7(d), it is seen that the variation of rolling-moment
coefficient with normal-force coefficient is quite erratic for the solid-
fin configuration; whereas in figure 8(d), it is seen that the slotted-
fin configuration experiences little or no rolling moment although there
is some scatter at the higher normal-force coefficients. The possibility
of asymmetric and erratic rolling characteristics occurring with long
body-tail configurations was discussed recently by Allen and Perkins in
reference 5. It was shown that the aperiodic discharge of vortices on
the lee side of a body might induce aperiodic asymmetric loads on the
stabilizing fins. Such an explanation is probably applicable to the
rolling moments of the present model at least for the solid-fin configu-
ration. It appears, however, that these erratic rolling tendencies are
suppressed in the case of the slotted-fin configuration.

DYNAMIC DAMPING-IN-ROLL CHARACTERISTICS

Range of Tests

Time histories of the roll position were recorded during the roll damping motions for angles of attack of -1°, 0°, 1°, 3°, and 5° at Mach numbers of 1.5, 1.7, and 1.9 utilizing both solid- and slotted-fin configurations and the HE head only. The initial roll velocity, p_o, was approximately 25 revolutions per second for all cases. Due to asymmetry of the model and/or tunnel air stream, the rocket assumed a constant autorotational velocity, p_a. Records of the autorotation velocity were taken for each of the test conditions and configurations listed above. Also recorded were the time histories of the roll damping motions for 0° angle of attack and zero wind velocity (wind-off) at various stagnation pressures starting at atmospheric pressure and approaching an absolute vacuum. These records were useful in determining friction effects as will be shown in the following section. All the wind-on roll data were obtained at a constant Reynolds number of 0.425×10^6.

Reduction of Data

The differential equation representing the damping of the free rolling motion can be written as

$$I_x \left(\frac{dp}{dt}\right) = pL_p + pF_p + A \tag{1}$$

where each term represents a rolling moment. It is assumed that the rolling moment due to friction is a linear function of the rolling angular velocity ($F_p = $ constant) and that the rolling moment due to asymmetry of the model and/or tunnel air stream is independent of time or roll velocity (A = constant).[1]

Equation (1) is a linear differential equation of the first order. The solution is

$$p = Ce^{kt} - \frac{A}{L_p + F_p} \tag{2}$$

---

[1] These assumptions apparently neglect the small residual moment due to friction inherent in any bearing; however, such a term is independent of rotational velocity and is considered as included in the asymmetry constant, A.

where C is a constant of integration and $k = (L_p + F_p)/I_x$. Setting the initial condition that $p = p_0$ at $t = 0$,

$$C = p_0 + \frac{A}{L_p + F_p}$$

Substituting in equation (2),

$$p = \frac{A}{L_p + F_p} (e^{kt} - 1) + p_0 e^{kt} \qquad (3)$$

The rolling moment due to asymmetry, A, can be taken into account by consideration of the autorotation condition. Setting p_a as the autorotation velocity, the equation representing this motion is given by equation (1) as dp/dt approaches zero, or

$$p_a L_p + p_a F_p + A = 0$$

Rearranging,

$$\frac{A}{L_p + F_p} = -p_a$$

Substituting in equation (3),

$$p = p_a (1 - e^{kt}) + p_0 e^{kt}$$

or

$$\frac{p - p_a}{p_0 - p_a} = e^{kt} \qquad (4)$$

It should be noted that when $p_a = 0$ the above equation reduces to the familiar

$$\frac{p}{p_0} = e^{kt}$$

Semilogarithmic plots of the rolling-angular-velocity ratio, $\dfrac{p - p_a}{p_0 - p_a}$, versus time should yield a straight line of slope equal to k.

In order to determine the damping-in-roll parameter, L_p, it remains to find the damping due to friction, F_p. Considering the wind-off time histories taken at various tunnel pressures, any aerodynamic damping can be eliminated by extrapolating to an absolute vacuum ($H = 0$). The

equation representing the rolling motion at $H = 0$ is

$$\frac{p}{p_o} = e^{(F_p/I_x)t}$$

Semilogarithmic plots of the rolling-angular-velocity ratio, p/p_o, versus time as before should yield a straight line of slope equal to F_p/I_x. Knowing k and using the extrapolated value of F_p/I_x at $H = 0$, the damping-in-roll parameter, L_p, is calculated from

$$L_p = I_x \left(k - \frac{F_p}{I_x}\right)$$

The damping-in-roll coefficient, C_{l_p}, may then be calculated as defined in the symbols.

Precision

The precision of the dynamic damping-in-roll data has been estimated from the known uncertainties involved, including errors in reading pressures, measurement of angles, time intervals, and weights of bodies. The following table lists the estimated uncertainty of the corresponding quantity:

Quantity	Uncertainty
Mach number	0.01
Reynolds number	0.03×10^6
Angle of roll, revolutions	0.025
Angle of attack, degrees	0.05
Time, seconds	0.001
Moment of inertia, lb-ft-sec^2	0.0003

The uncertainties listed above are maximum values, but in most cases the uncertainty is somewhat less.

Results and Discussion

Basic experimental data plots of the rolling-angular-velocity ratio, $\dfrac{p-p_a}{p_o-p_a}$, as a function of time are presented in semilogarithmic

form in figures 9 and 10 for the solid- and slotted-fin configurations, respectively. Presentation of the results in this form provides a convenient method of reducing the data, since, as discussed earlier, the slope so obtained is constant. Although the semilogarithmic plots of figures 9 and 10 have constant slopes over most of the damping period, there is some change of slope at the lower rolling-angular-velocity ratios. The effect of the change in slope is a negligible one, however, since similar changes of slope were noted in the plots of the wind-off damping motions shown in figures 11 and 12 and may safely be assumed to be a friction effect rather than an aerodynamic one. The slopes used in the subsequent calculations are those at angular-velocity ratios of 0.3 or more where the slope is constant.

The slopes of the wind-off damping motions are shown in figure 13 as a function of the tunnel total pressure. The extrapolated value of these slopes at zero pressure produces the damping due to friction, $F_p/I_x = -0.094$ per second.

The slopes of figures 9 and 10 have been corrected for the friction term, F_p/I_x, and reduced to coefficient form as outlined in the section entitled "Reduction of Data"; the results are shown in figure 14. There appears to be very little difference in the damping-in-roll coefficient between solid and slotted fins at $M = 1.5$ within the angle-of-attack range tested; however, the damping-in-roll coefficients for the slotted-fin configuration are approximately 10 to 25 percent less than those for the solid fins at Mach numbers of 1.7 and 1.9. It is interesting to note that the damping-in-roll coefficients for the solid fins seem to vary somewhat with angle of attack, whereas the damping-in-roll coefficients for the slotted fins are more nearly constant with angle of attack.

Another interesting comparison is shown in figure 15. The damping-in-roll coefficients for both the solid- and slotted-fin configurations at zero angle of attack as a function of effective aspect ratio, βAR, are shown in comparison with the damping-in-roll coefficients of rectangular wings as given by linear theory (reference 6) neglecting the effects of the body.[2] The agreement for the solid-fin configuration is excellent, whereas the slotted-fin values are approximately 15 to 25 percent less than that given by theory for solid fins. As an approximation procedure, if the damping-in-roll coefficients given by linear

[2]An approximation method for determining the damping in roll of rectangular wing-body combinations is given in reference 7; however, the method is not applicable to the effective aspect ratios of the present investigation due to limitations of the method.

theory were reduced by an amount equivalent to the percent reduction in exposed-fin area (21 percent) due to the slots, the slotted-fin damping-in-roll coefficients, as well as the solid-fin damping-in-roll coefficients, can be predicted with a good degree of accuracy by linear-theory methods.

CONCLUDING REMARKS

The results of the experimental investigation of the static aerodynamic and dynamic damping-in-roll characteristics of the 8-cm aircraft rocket can be summarized as follows:

1. The rocket was found to be statically stable at M = 0.7 and 1.7 when fitted with either solid or slotted fins.

2. The normal-force and pitching-moment coefficients of the slotted-fin configuration were reduced from solid-fin values by an amount approximately commensurate with the reduction in area due to the slots.

3. Axial-force coefficients of the slotted-fin configuration were increased about 15 percent over solid-fin values (M = 0.6 to 0.92 and 1.2 to 1.7).

4. Normal-force and pitching-moment coefficients of the rocket with either solid or slotted fins were unchanged with roll position.

5. The rocket exhibited very erratic rolling moments at various roll positions when fitted with solid fins, especially at high angles of attack. However, the slotted-fin configuration appeared to suppress any adverse rolling tendencies and exhibited little or no rolling moment at any roll position (M = 1.7).

6. The damping-in-roll coefficients of the solid-fin configuration at 0° angle of attack were found to be equivalent to those predicted by linear theory for thin rectangular wings of the same effective aspect ratio, βAR. The damping-in-roll coefficients of the slotted-fin configuration varied from 15 to 25 percent less than that predicted by linear theory neglecting the effect of the slots (M = 1.5 to 1.9).

7. The damping-in-roll coefficients of the solid-fin configuration varied approximately 20 percent up to angles of attack of 5°, whereas the damping-in-roll coefficients of the slotted-fin configuration were relatively constant with angle of attack (M = 1.5 to 1.9).

On the basis of the foregoing results it appears that the principal advantage to be gained by the use of slotted fins, as opposed to solid

fins, is the suppression of the adverse rolling tendencies associated with long body-fin arrangements where the fins are situated far aft on the body. In the present case the rocket is spin stabilized and this characteristic is not so important unless the rocket is fired at long range and the spin velocity becomes too low; however, for long body-fin arrangements where roll stabilization is desired, the use of slots may provide an adequate means of overcoming any adverse rolling tendencies.

The good agreement obtained between the experimental damping-in-roll coefficients of the rocket and that given by linear theory for wings indicates that even for fins mounted behind a long forebody, the damping in roll can be predicted by linear-theory methods with a good degree of accuracy.

Ames Aeronautical Laboratory
    National Advisory Committee for Aeronautics
        Moffett Field, Calif.

REFERENCES

1. Frick, Charles W., and Olson, Robert N.: Flow Studies in the Asymmetric Adjustable Nozzle of the Ames 6- by 6-Foot Supersonic Wind Tunnel. NACA RM A9E24, 1949.

2. Edwards, S. Sherman: Experimental and Theoretical Study of Factors Influencing the Longitudinal Stability of an Air-to-Air Missile at a Mach Number of 1.4. NACA RM A51J19, 1952.

3. Perkins, Edward W.: Experimental Investigation of the Effects of Support Interference on the Drag of Bodies of Revolution at a Mach Number of 1.5. NACA TN 2292, 1951.

4. Herriot, John G.: Blockage Corrections for Three-Dimensional-Flow Closed-Throat Wind Tunnels, with Consideration of the Effect of Compressibility. NACA Rep. 995, 1950. (Formerly NACA RM A7B28)

5. Allen, H. Julian, and Perkins, Edward W.: Characteristics of Flow Over Inclined Bodies of Revolution. NACA RM A50L07, 1951.

6. Harmon, Sidney M.: Stability Derivatives at Supersonic Speeds of Thin Rectangular Wings with Diagonals Ahead of Tip Mach Lines. NACA Rep. 925, 1949. (Formerly NACA TN 1706)

7. Tucker, Warren A., and Piland, Robert O.: Estimation of the Damping in Roll of Supersonic-Leading-Edge Wing-Body Combinations. NACA TN 2151, 1950.

Figure 1.- Photograph of the 8-cm aircraft rocket mounted in the Ames 6- by 6-foot supersonic wind tunnel.
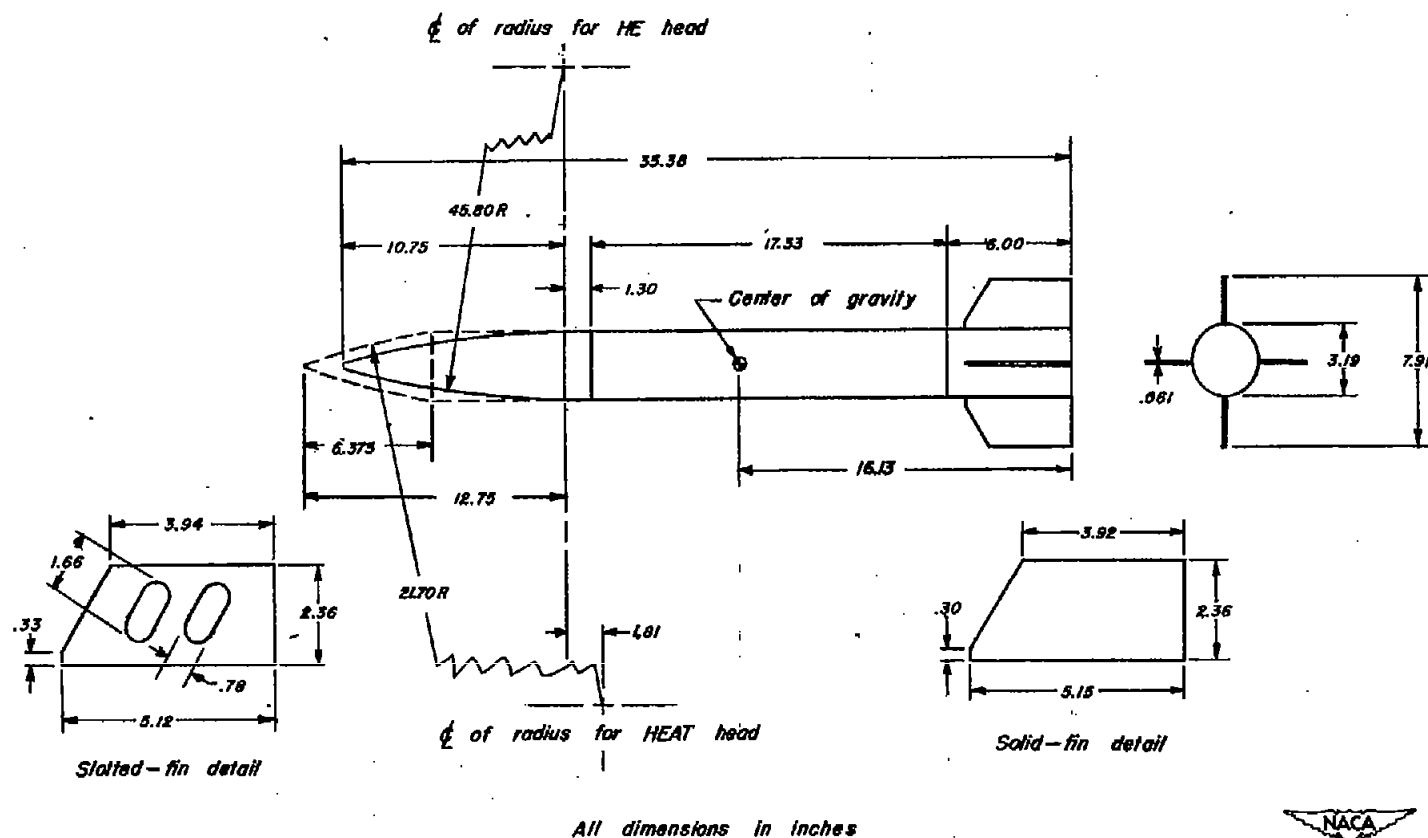
Figure 2.— Geometric characteristics of the 8-cm aircraft rocket.
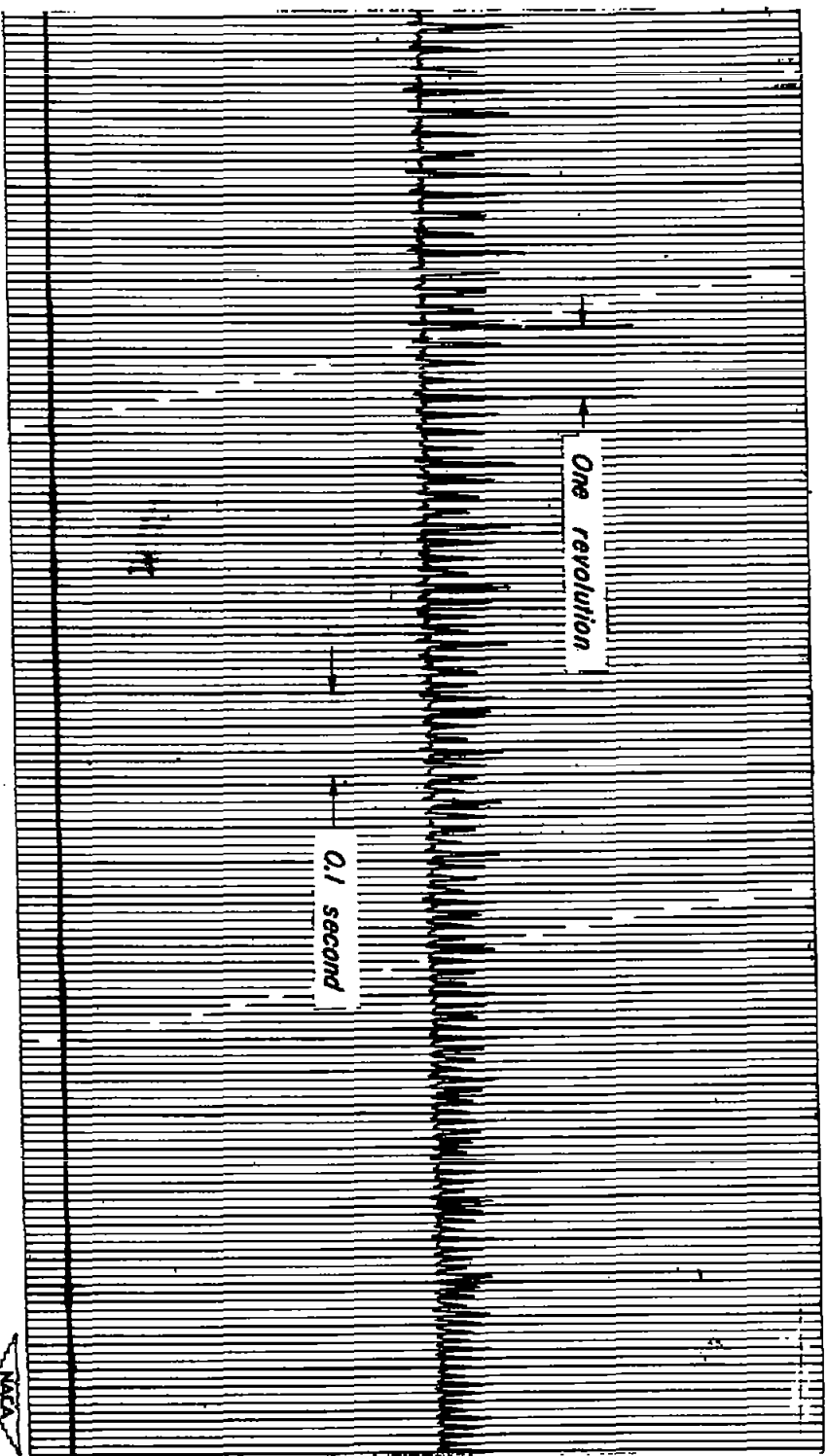
Figure 3.— Sample oscillograph record of a typical time history of the roll position for the 8-cm aircraft rocket.
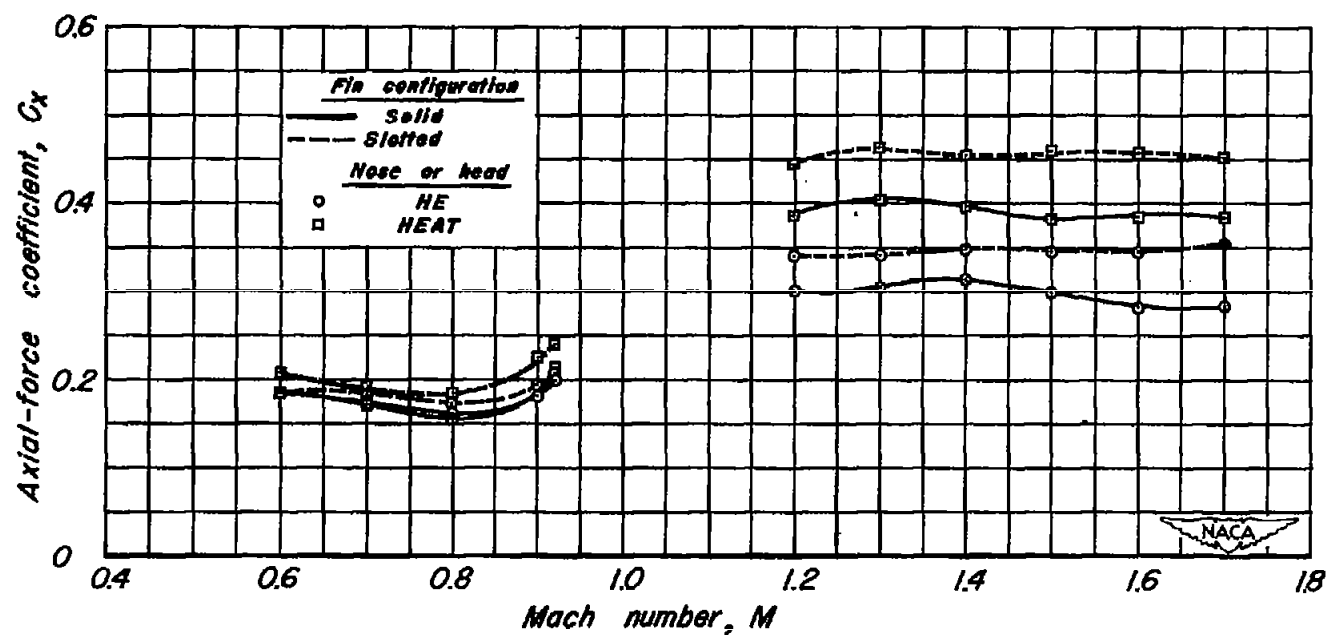
Figure 4.- Variation of axial-force coefficient with Mach number for the 8-cm aircraft rocket at $\alpha = 0.^{\circ}$
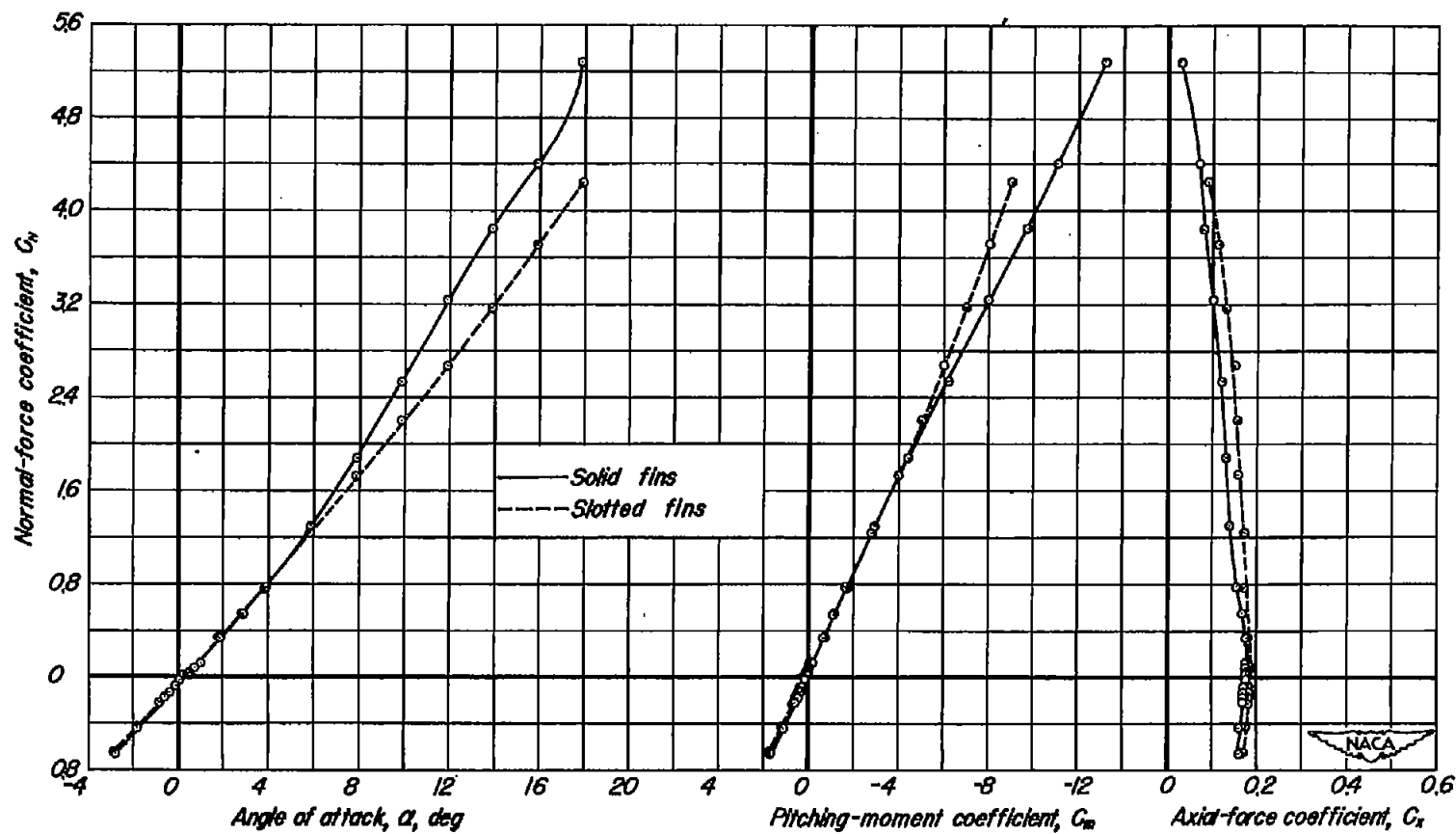
(a) M=0.7

Figure 5.- Static aerodynamic characteristics of the 8-cm aircraft rocket fitted with the high-explosive (HE) head.
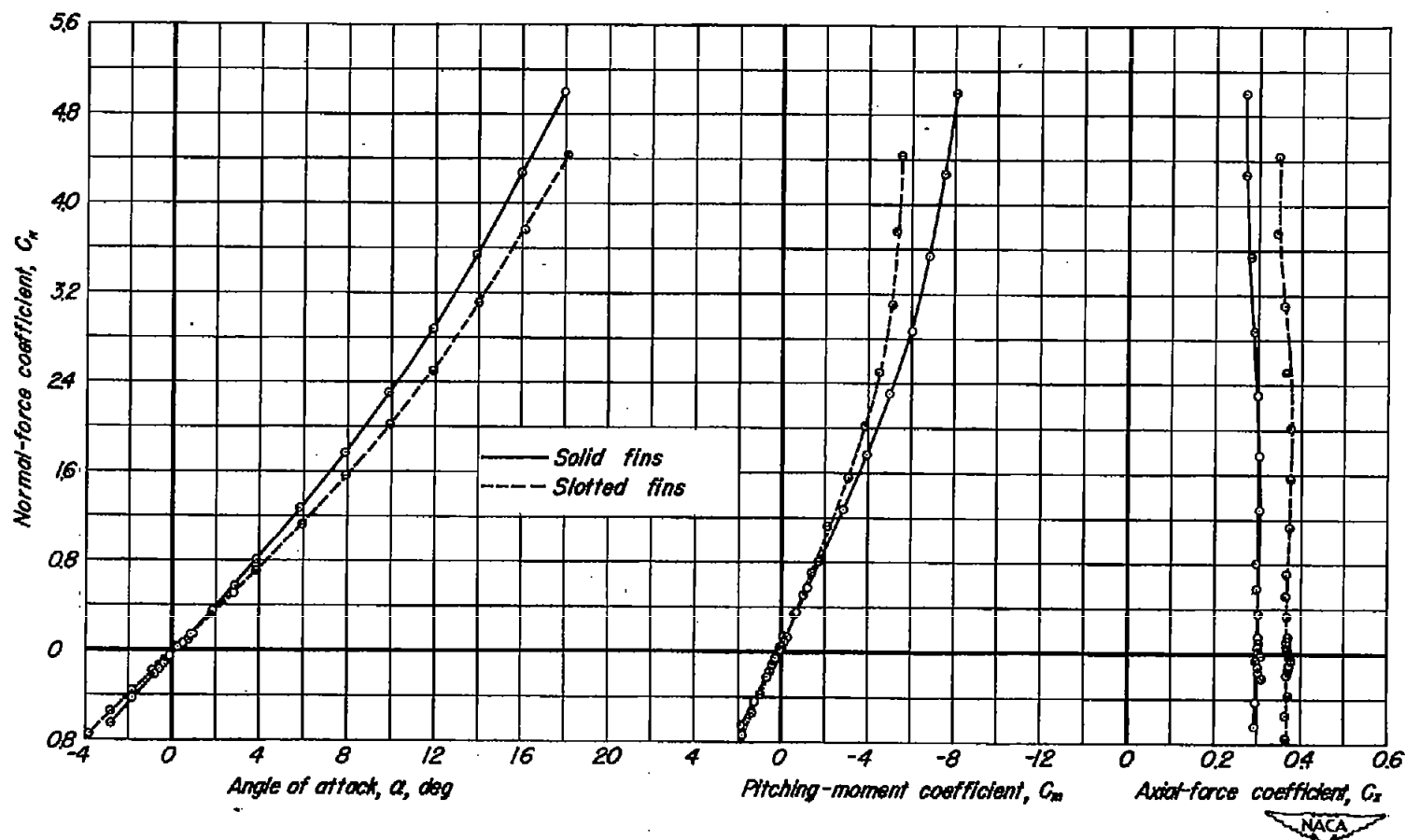
(b) M = 1.7

Figure 5. - Concluded.

Solid fins
Slotted fins
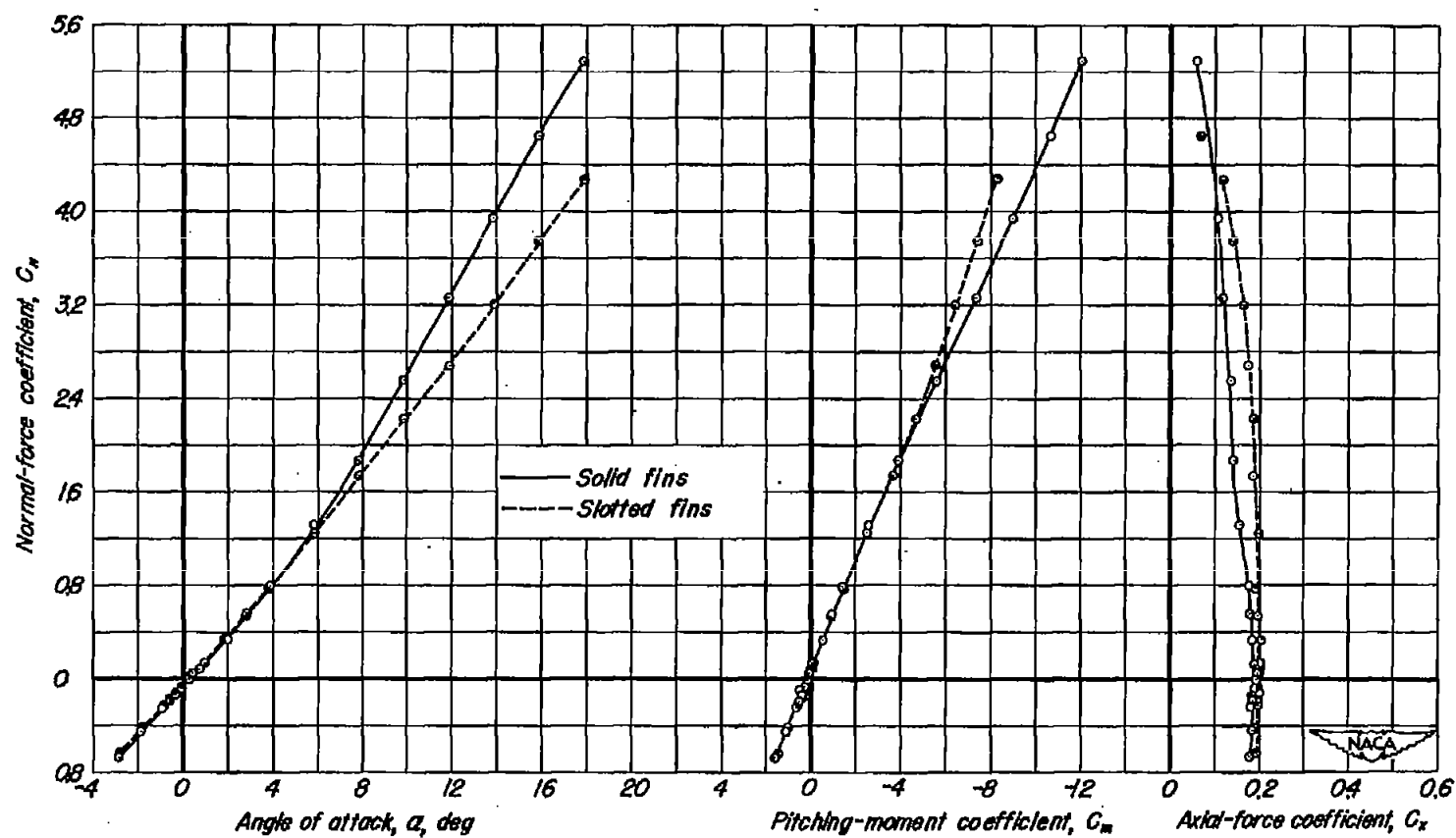
(a) M=0.7

Figure 6.- Static aerodynamic characteristics of the 8-cm aircraft rocket fitted with the high-explosive, antitank (HEAT) head.
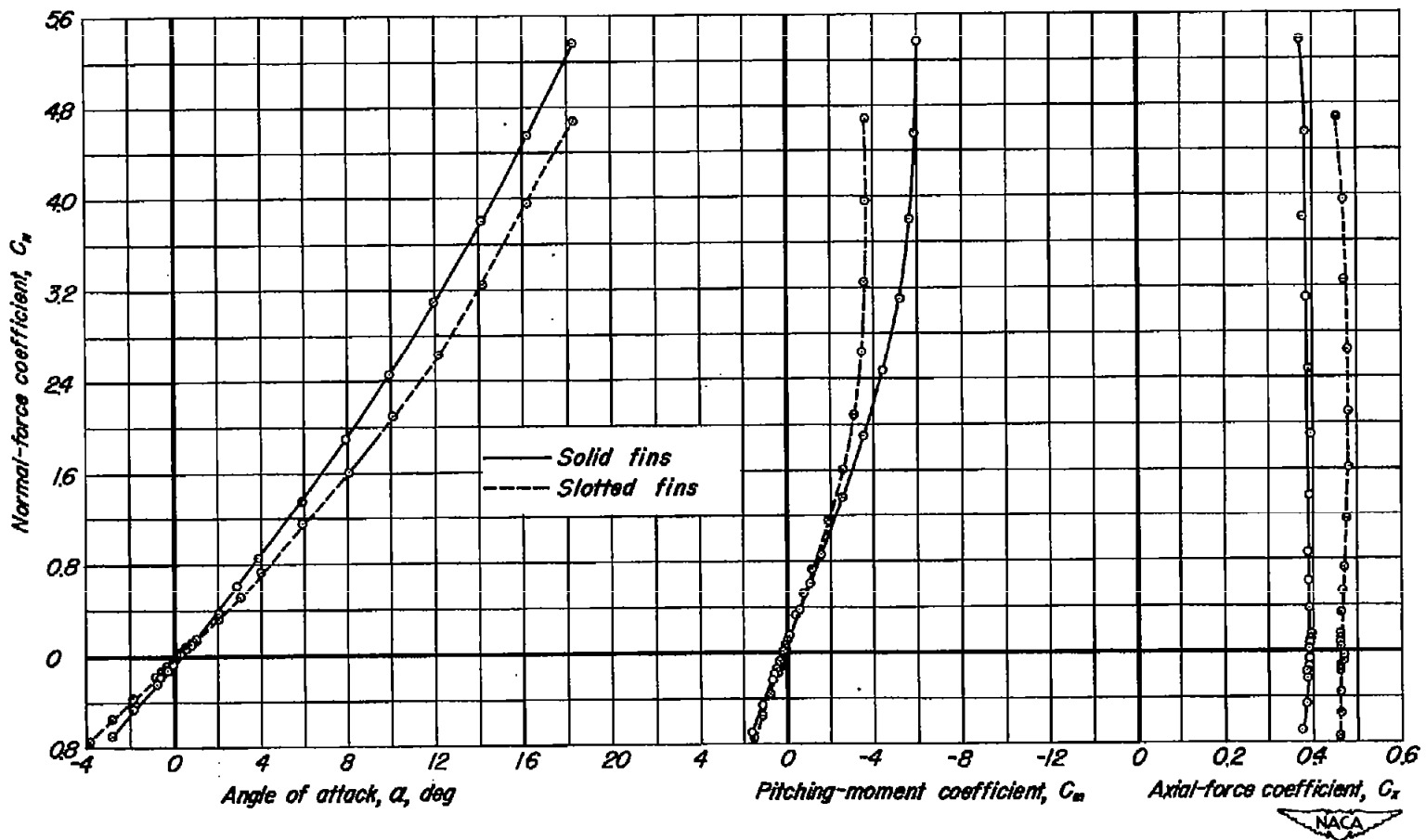
(b) M=1.7

Figure 6.- Concluded.
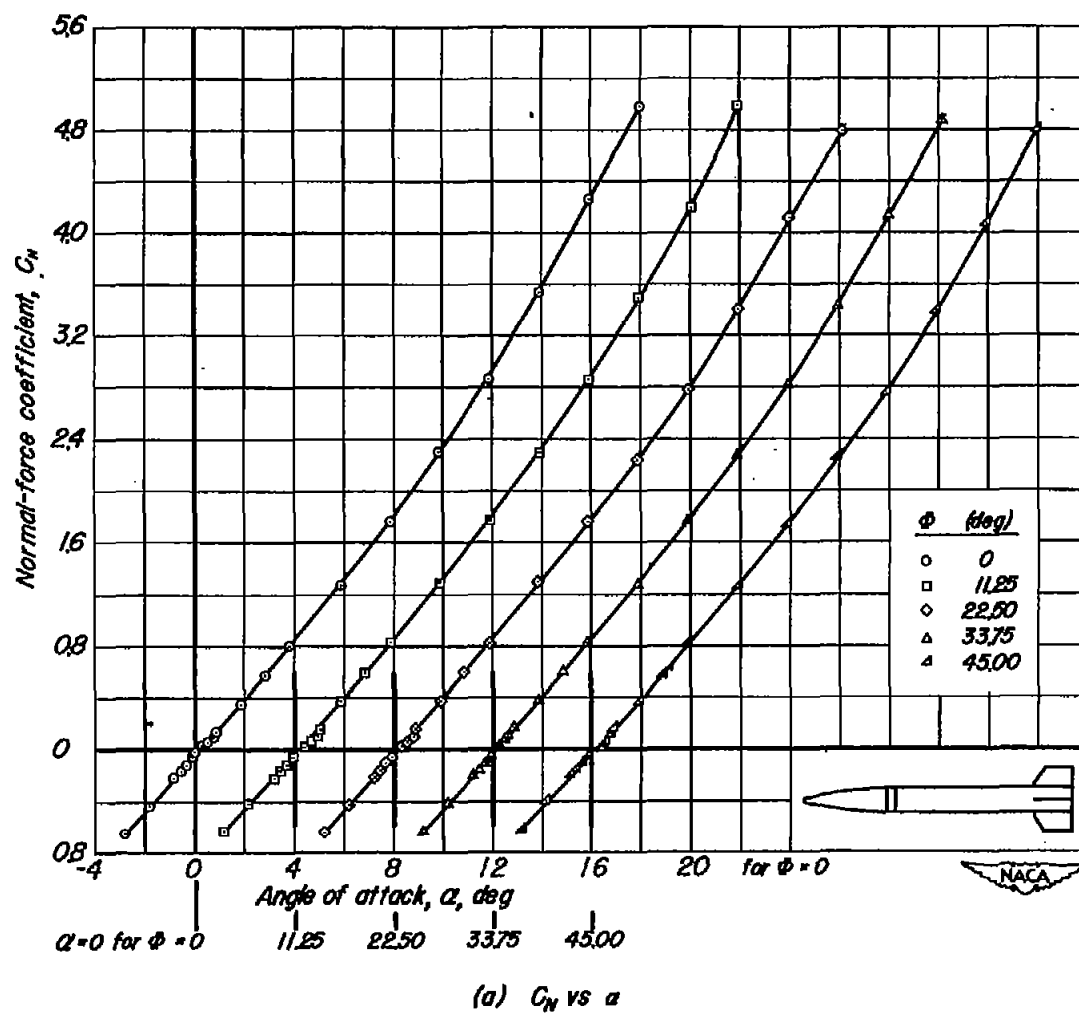
(a) C_N vs α

Figure 7.- Static aerodynamic characteristics of the 8-cm aircraft
rocket fitted with solid fins and high-explosive (HE) head at
various angles of roll and $M = 1.7$.
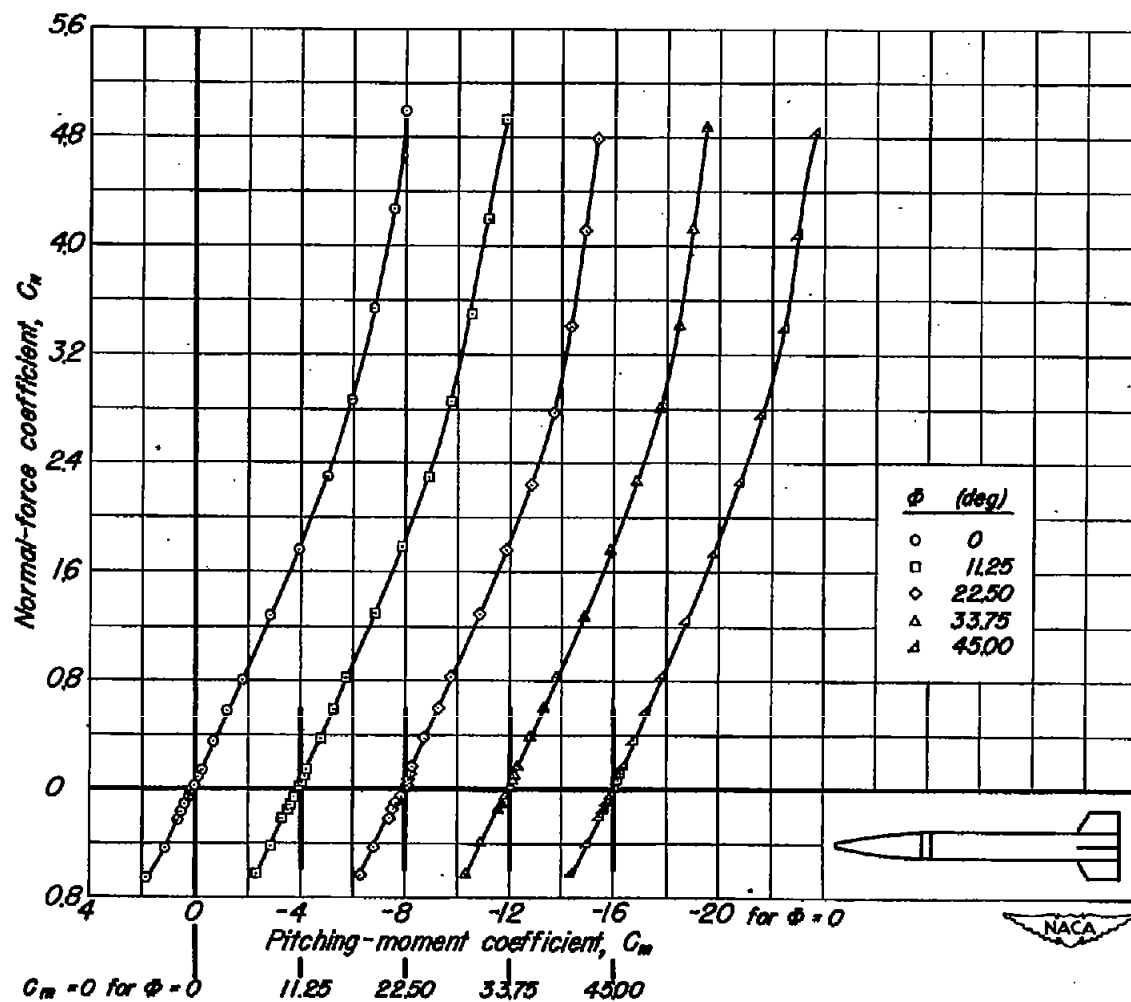
(b) C_m vs C_N

Figure 7.— Continued.

(c) C_X vs C_N

Figure 7.- Continued.

(d) C_l vs C_N
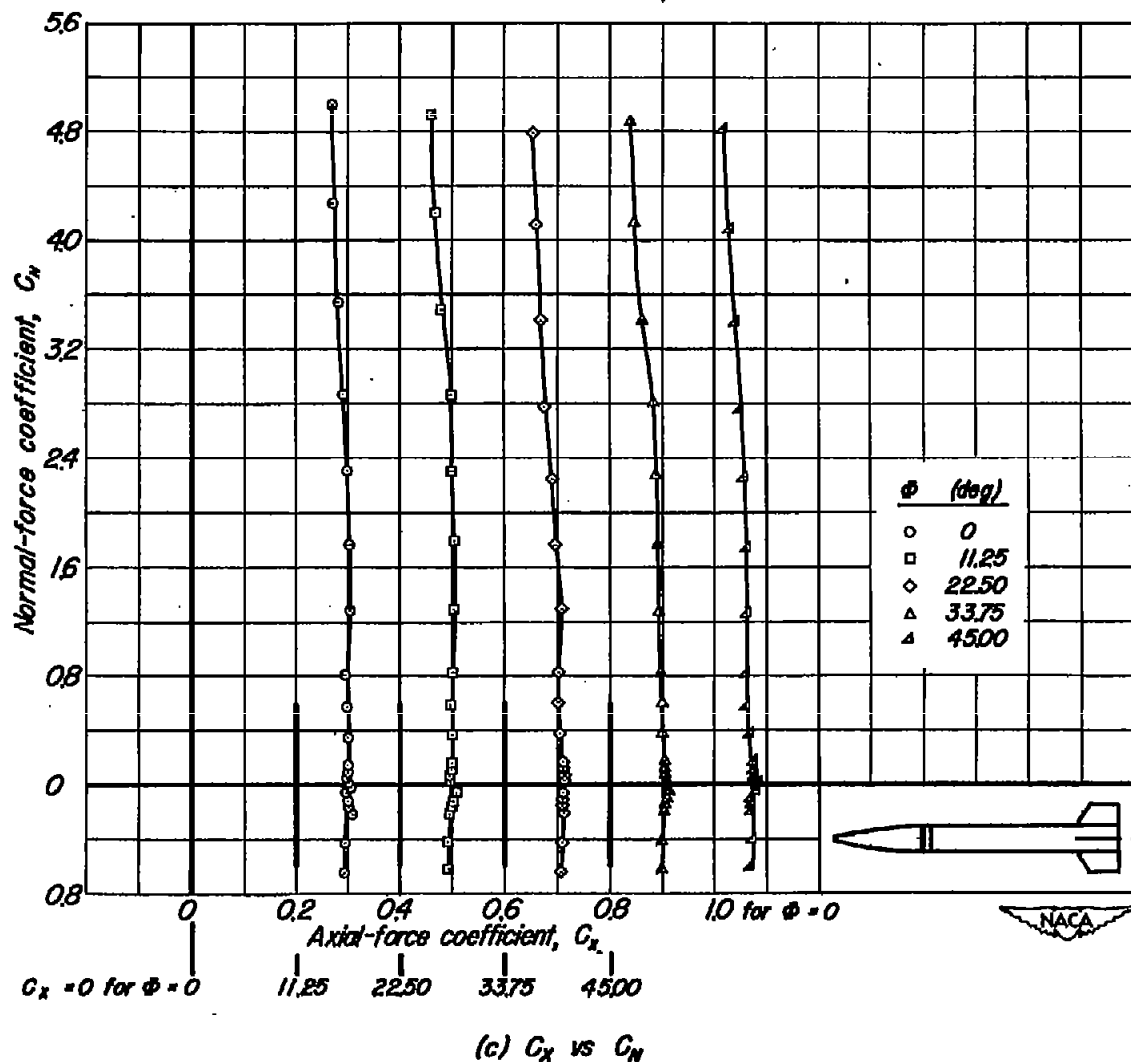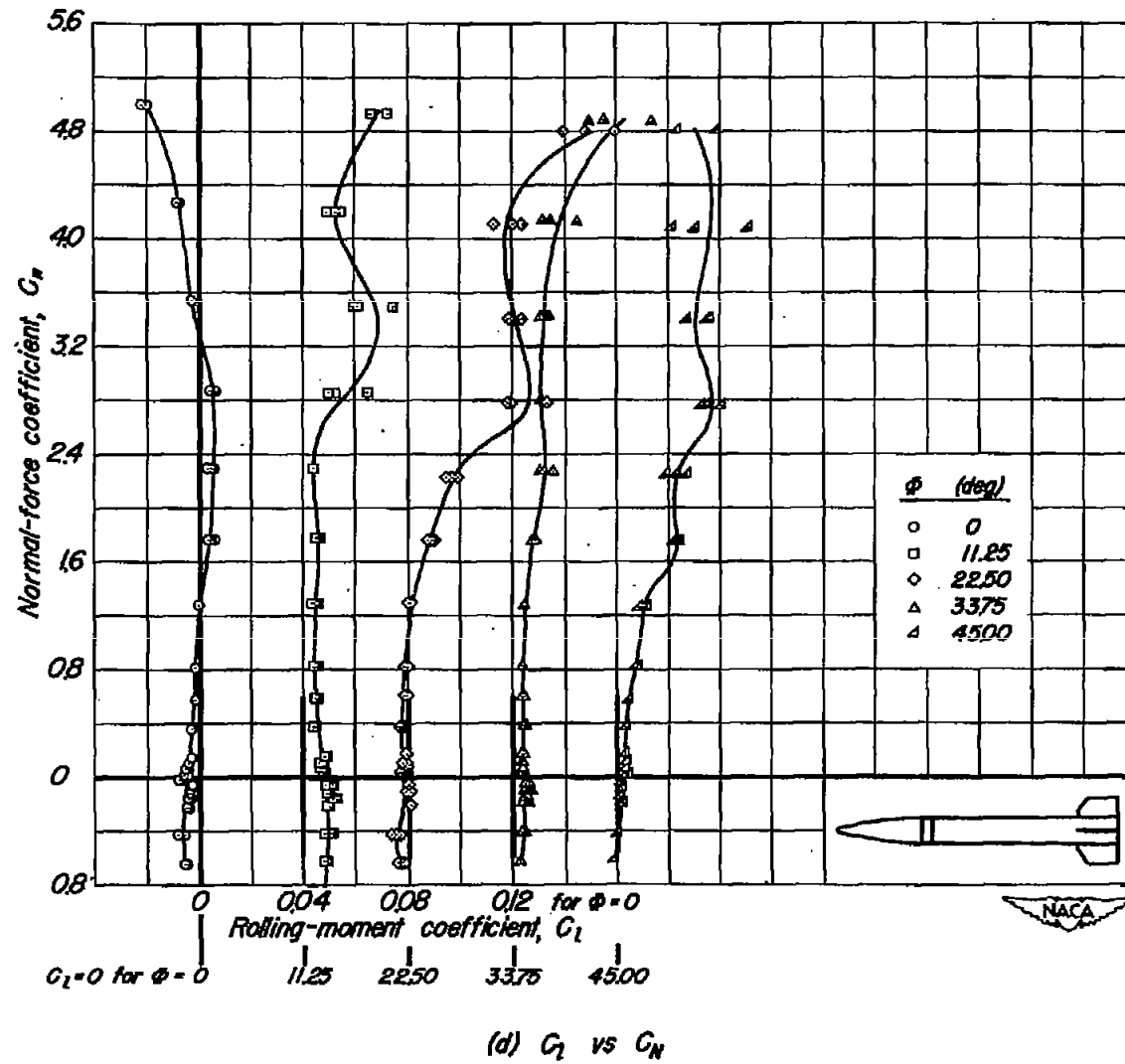
Figure 7.- Concluded.
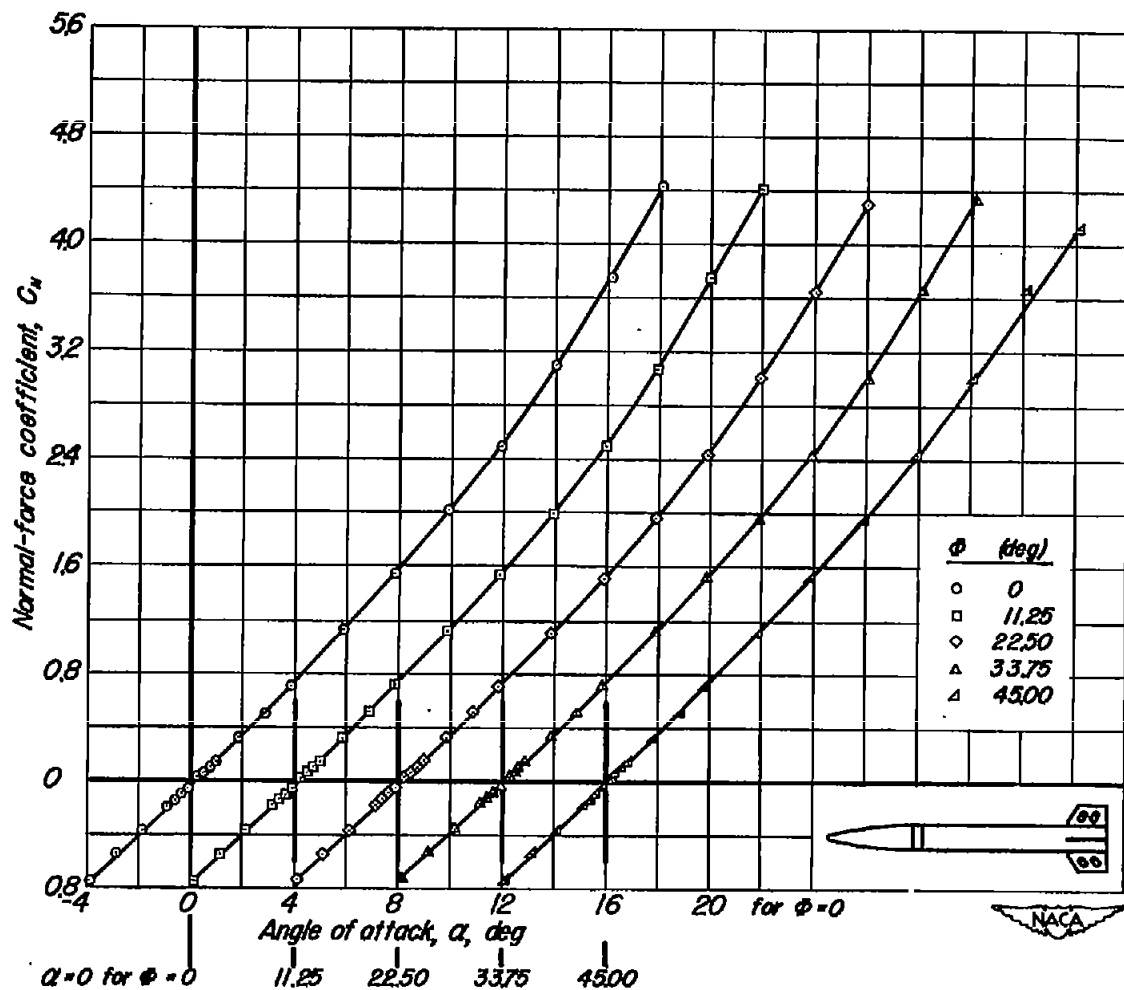
(a) C_N vs α

Figure 8.- Static aerodynamic characteristics of the 8-cm aircraft
rocket fitted with slotted fins and high-explosive (HE) head at
various angles of roll and $M = 1.7$.

(b) C_m vs C_N

Figure 8.- Continued.

Φ (deg)
○ 0
□ 11.25
◇ 22.50
△ 33.75
△ 45.00

$C_x = 0$ for $\Phi = 0$ 11.25   22.50   33.75   45.00
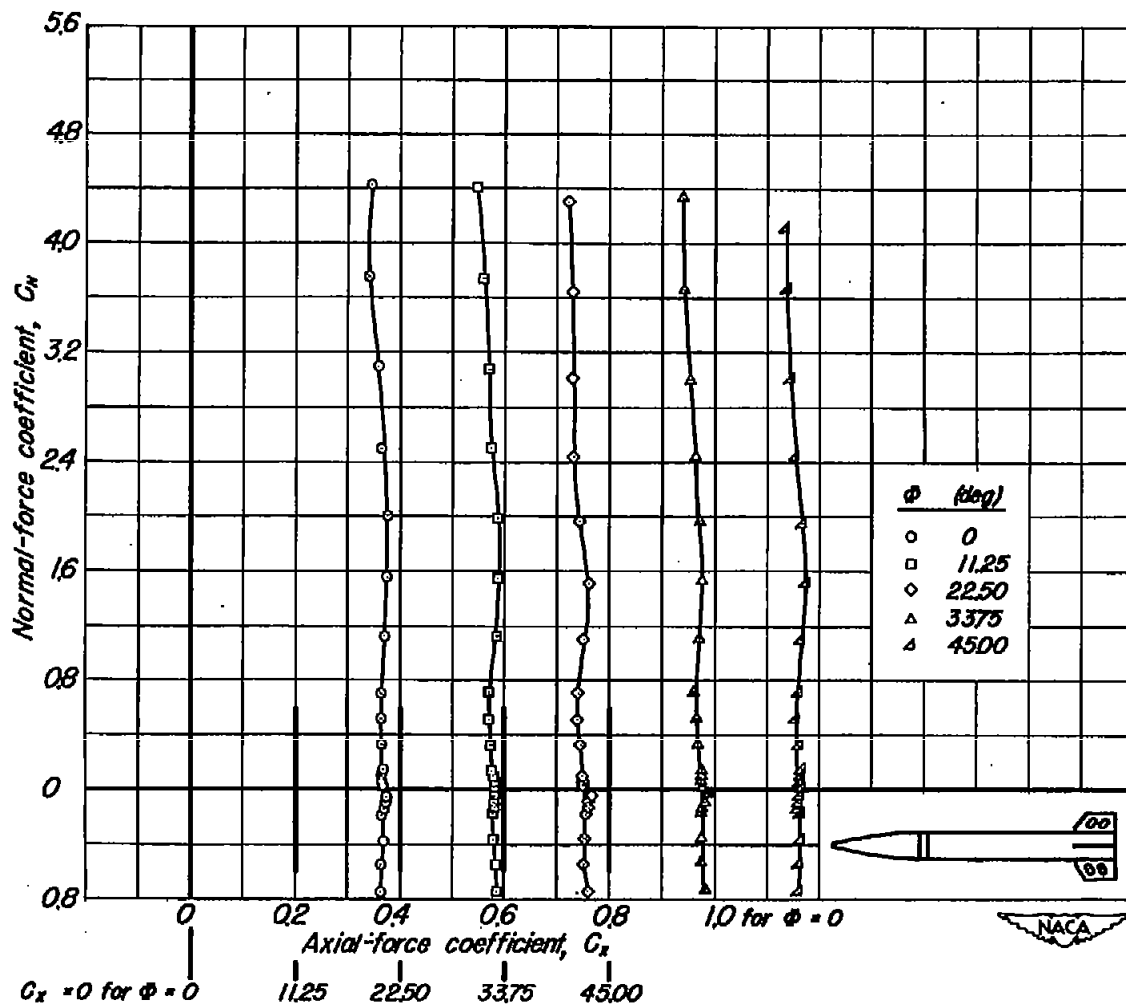
(c) C_x vs C_N
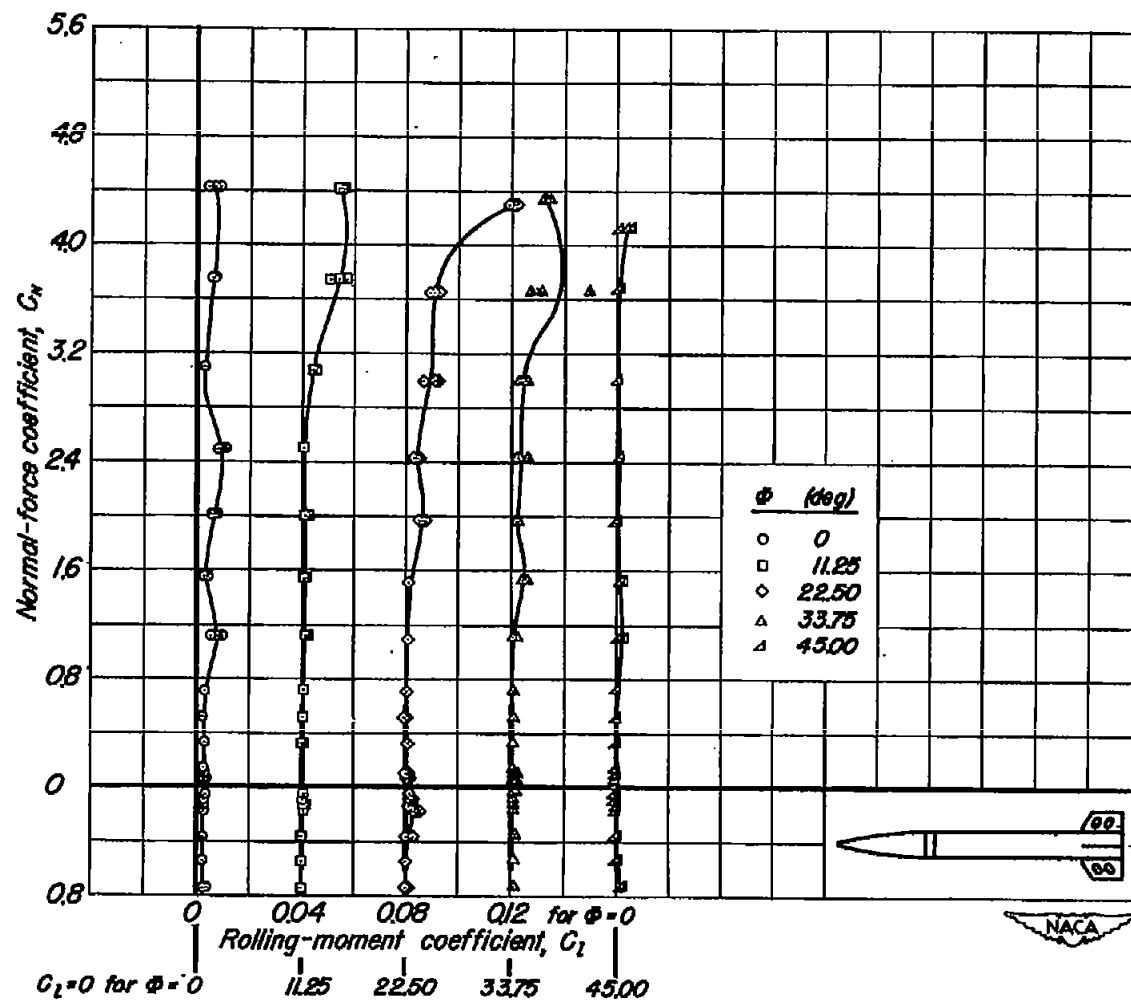
Figure 8.- Continued.

(d) C_l vs C_N

Figure 8.- Concluded.
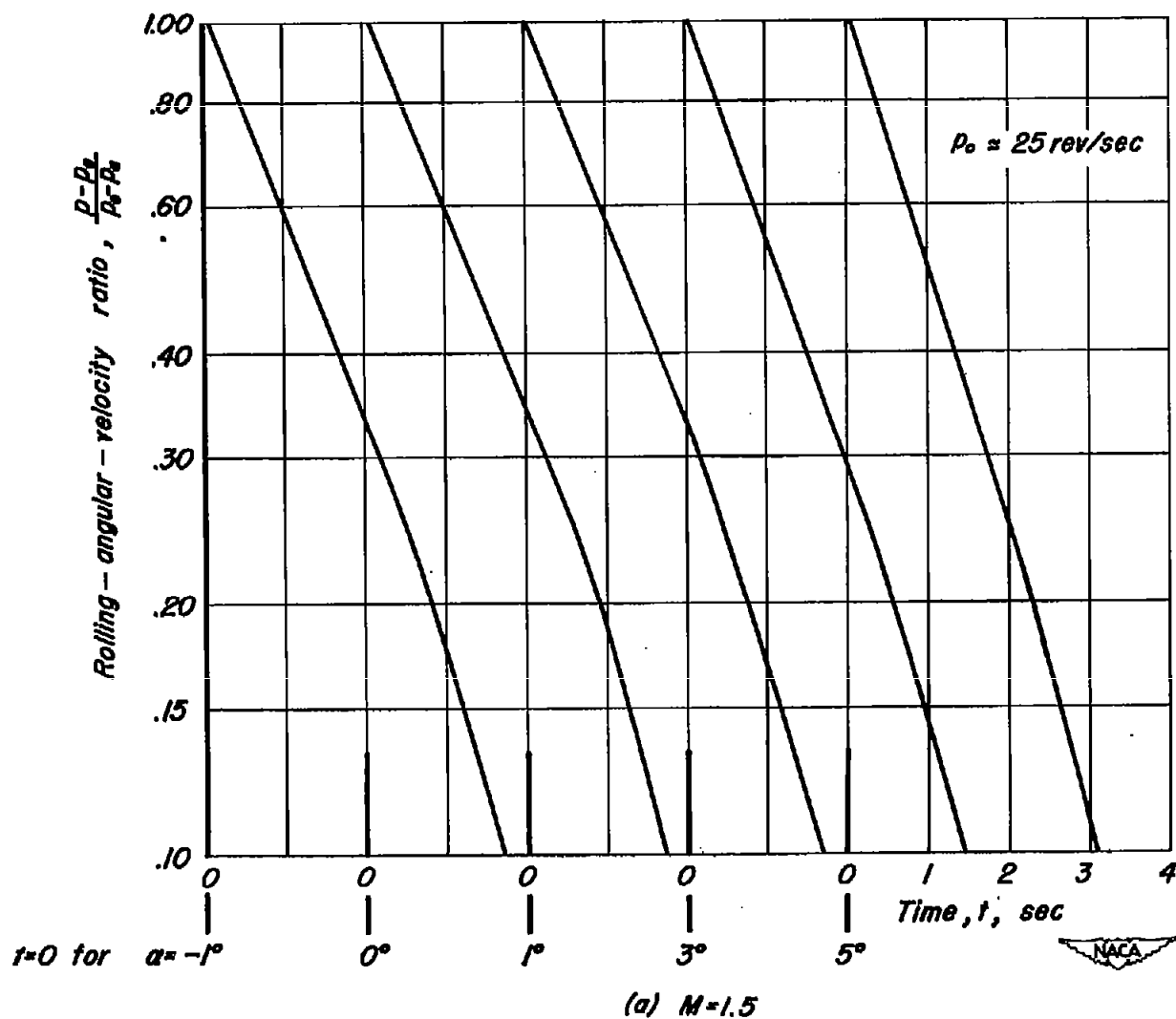
(a) M = 1.5

Figure 9. — Time histories of the rolling-angular-velocity ratio, $\frac{p-p_a}{p_s-p_a}$, for the solid-fin configuration.
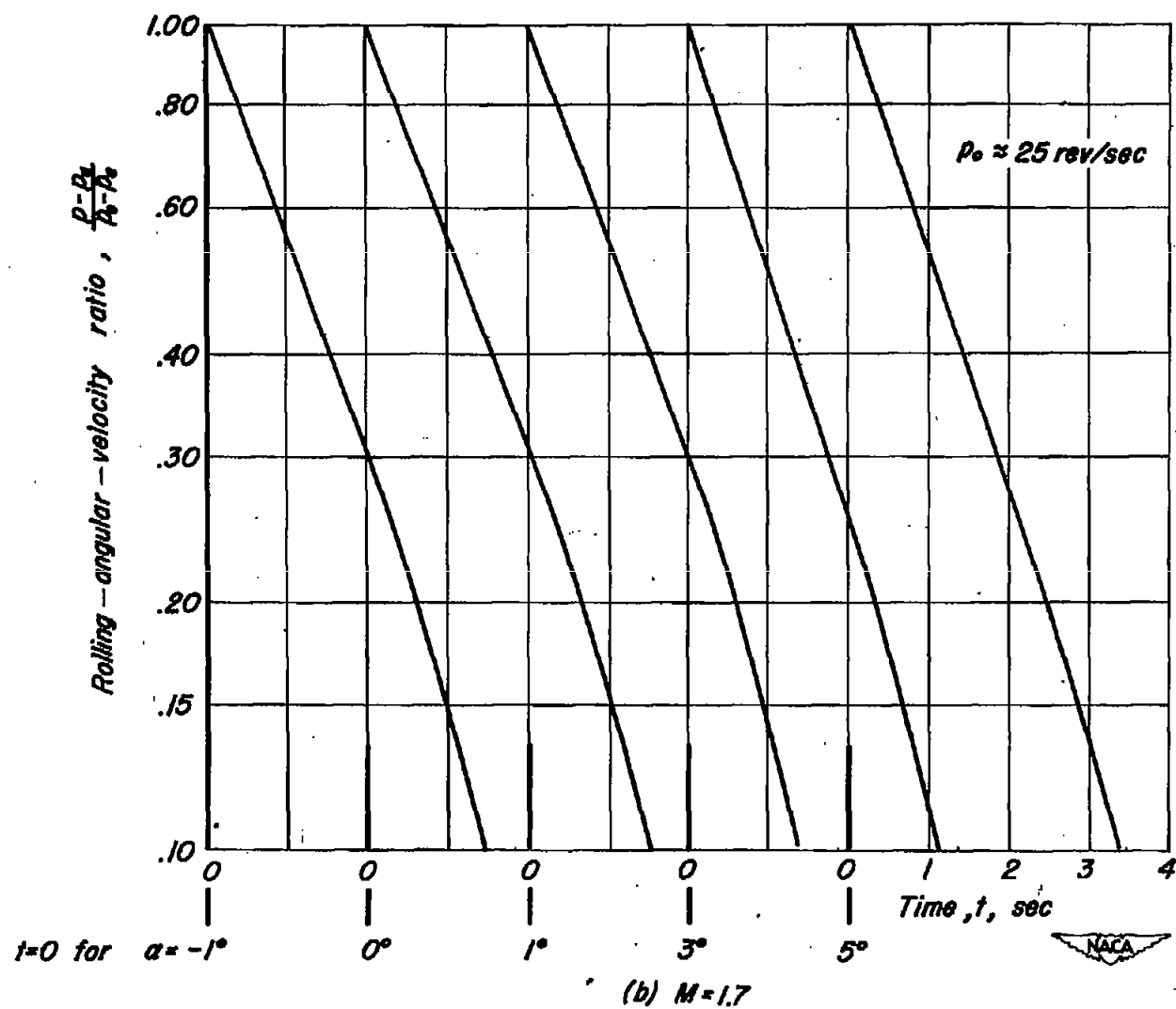
(b) M = 1.7

Figure 9. - Continued.
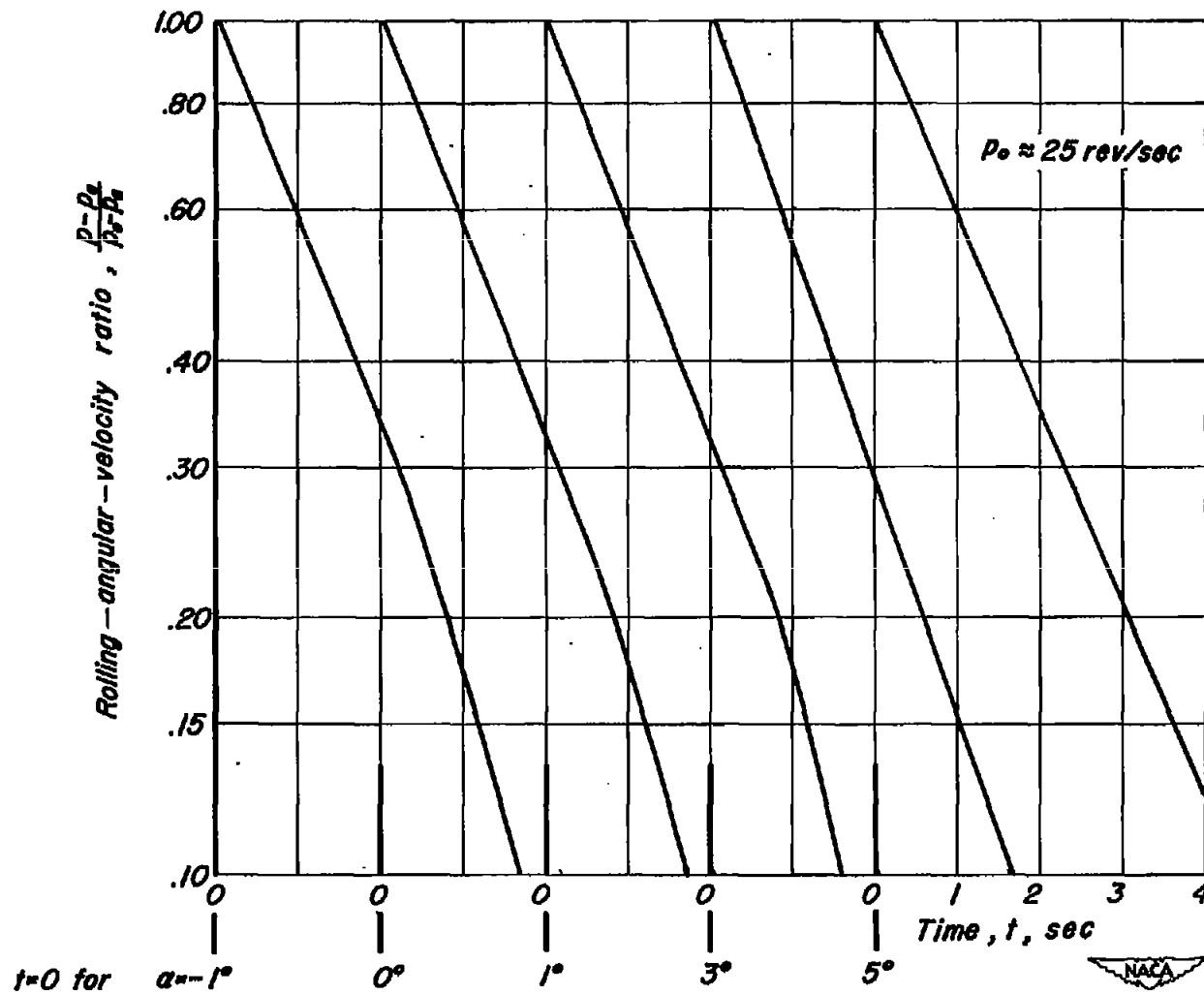
(c) $M = 1.9$

Figure 9. – Concluded.
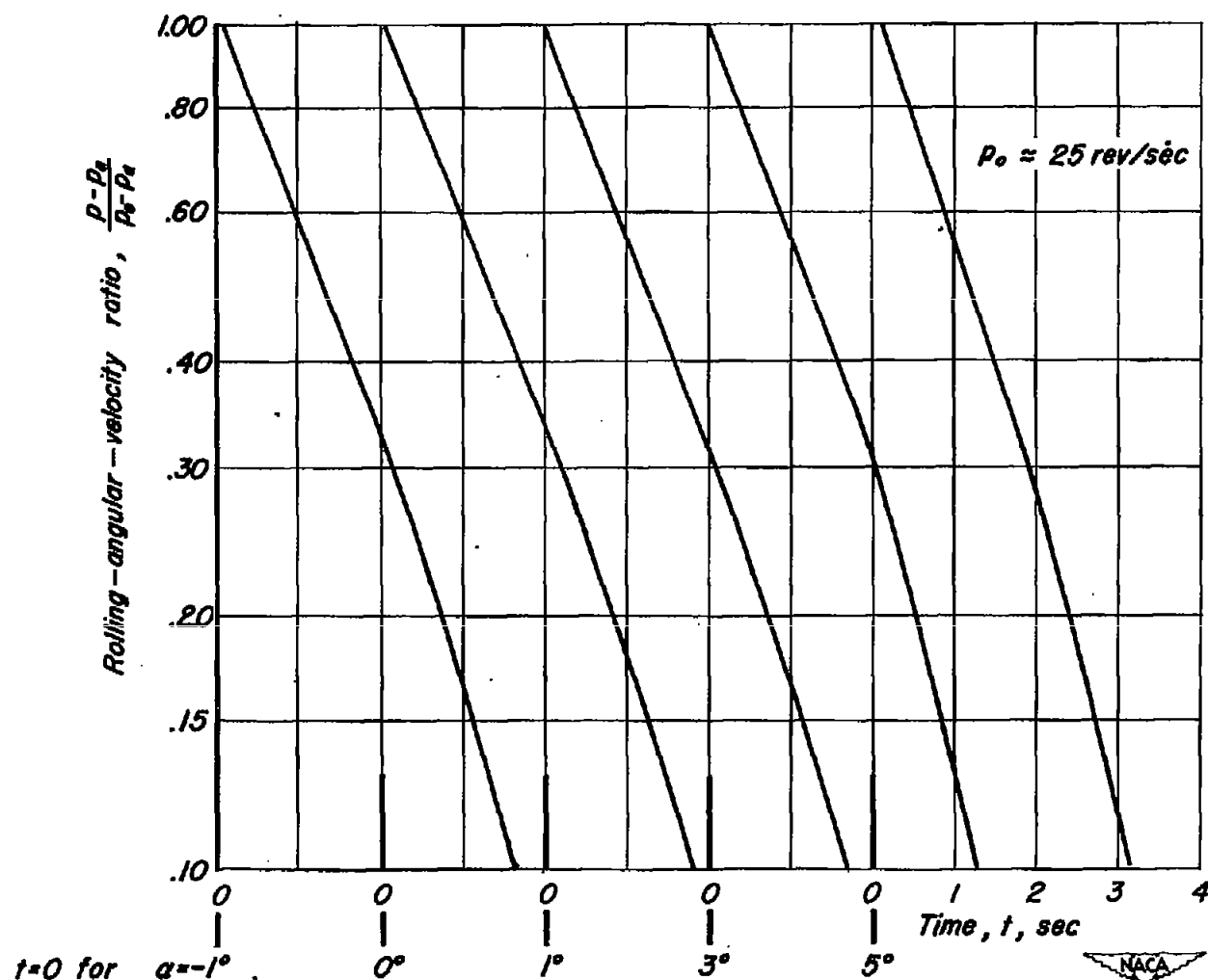
(a) M=1.5

Figure 10. — Time histories of the rolling-angular-velocity ratio, $\frac{p-p_4}{p_0-p_4}$, for the slotted-fin configuration.
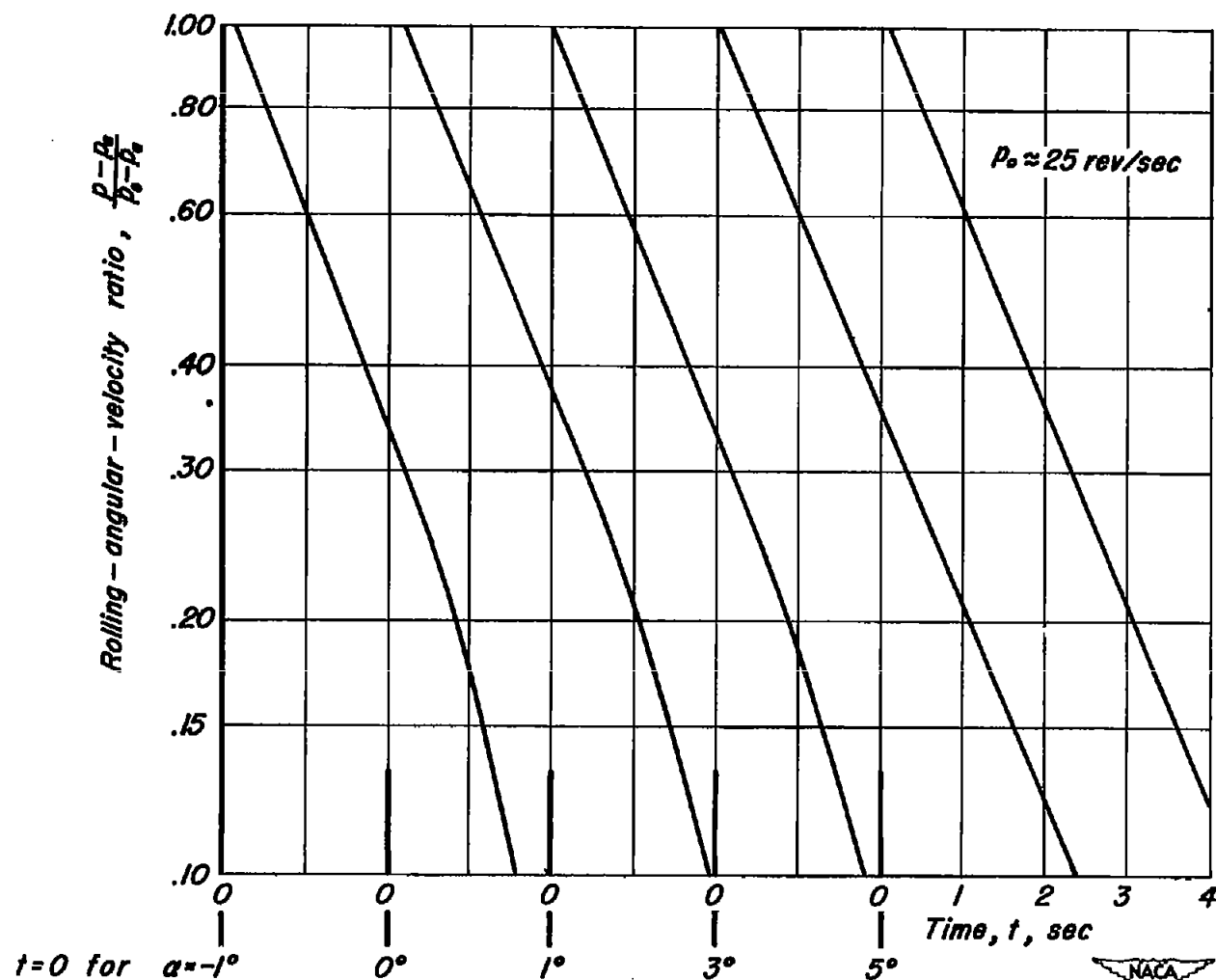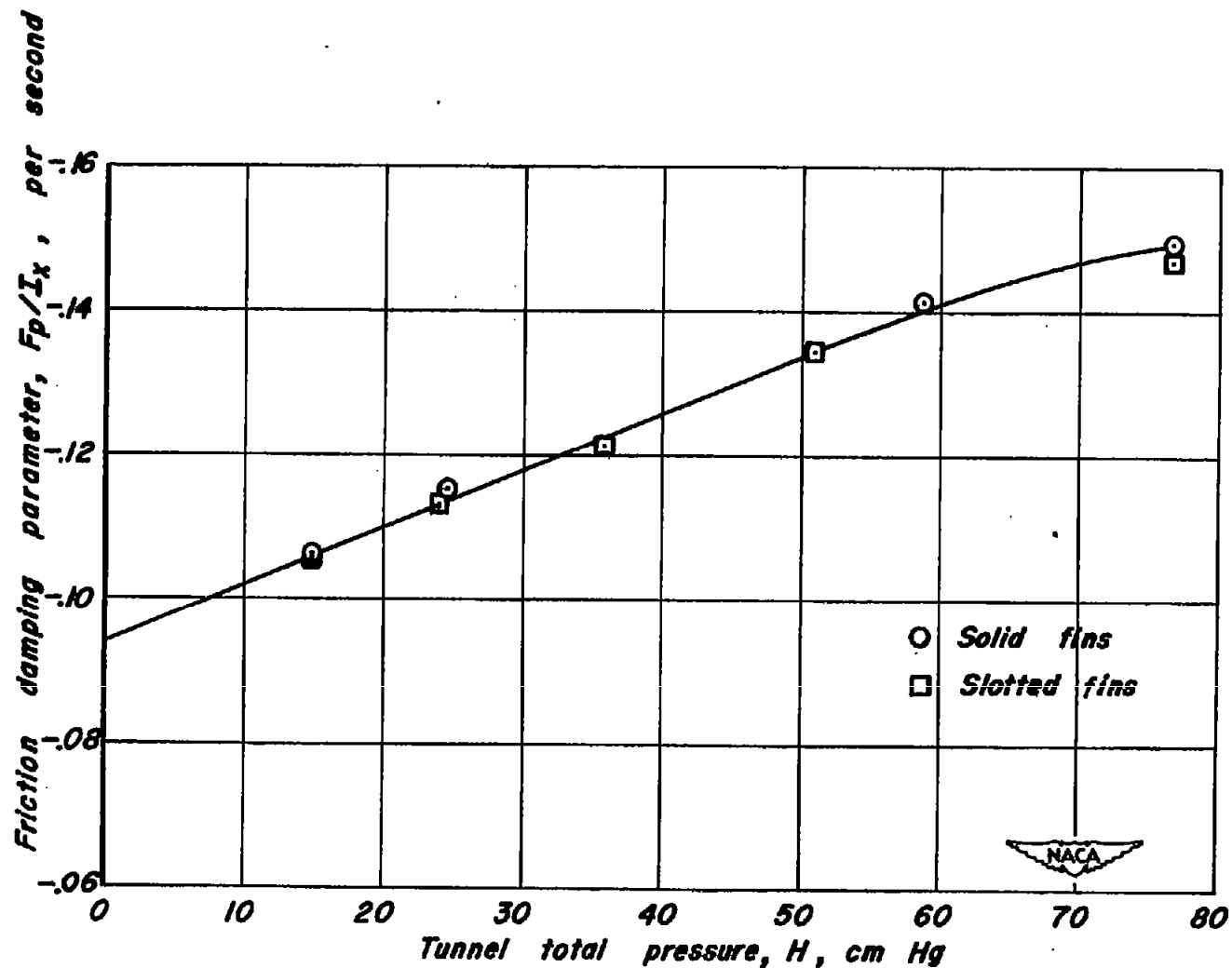
(b) M = 1.7

Figure 10. — Continued.
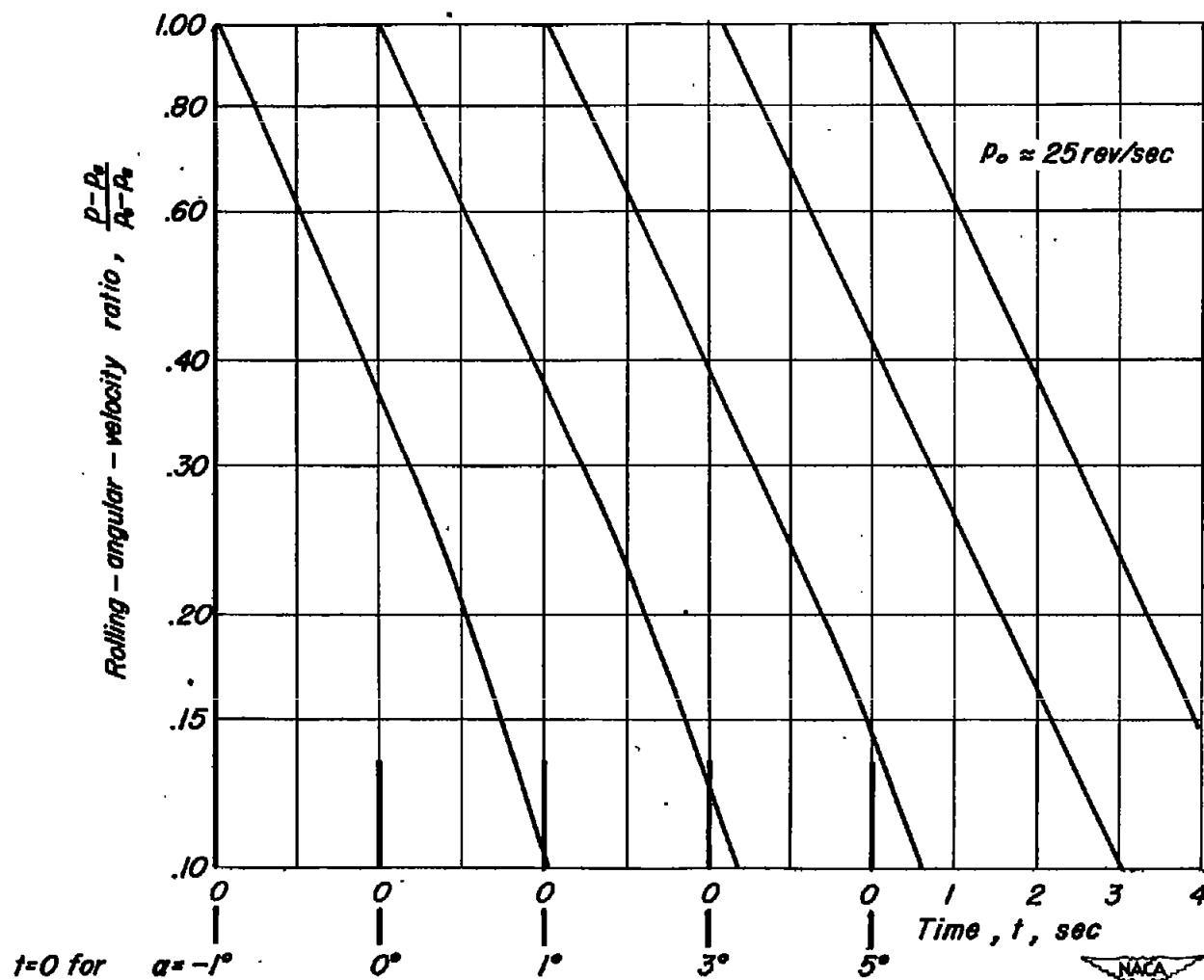
(c) M = 1.9

Figure 10.— Concluded.
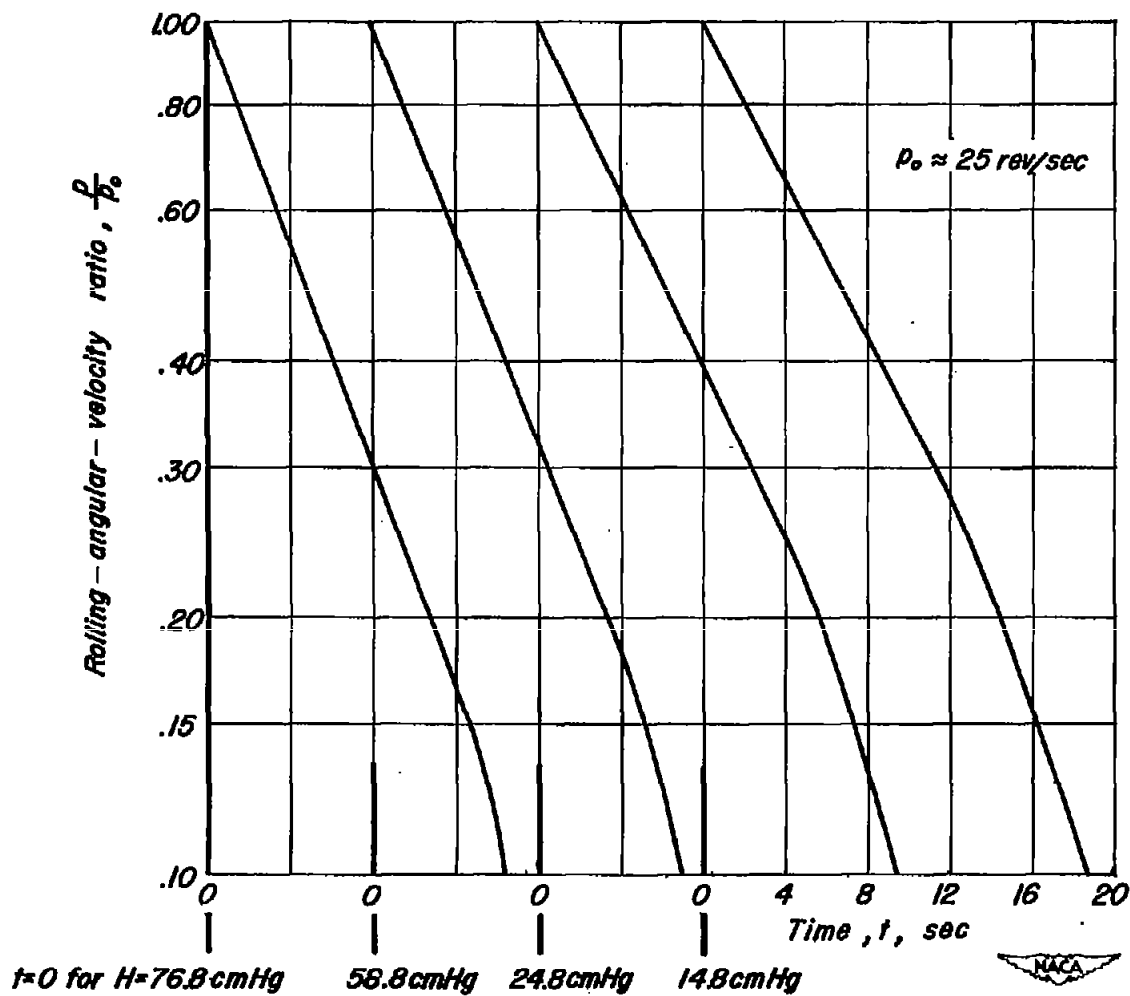
Figure 11. — Wind-off time histories of the rolling-angular-velocity ratio, $\frac{p}{p_o}$, for the solid-fin configuration.
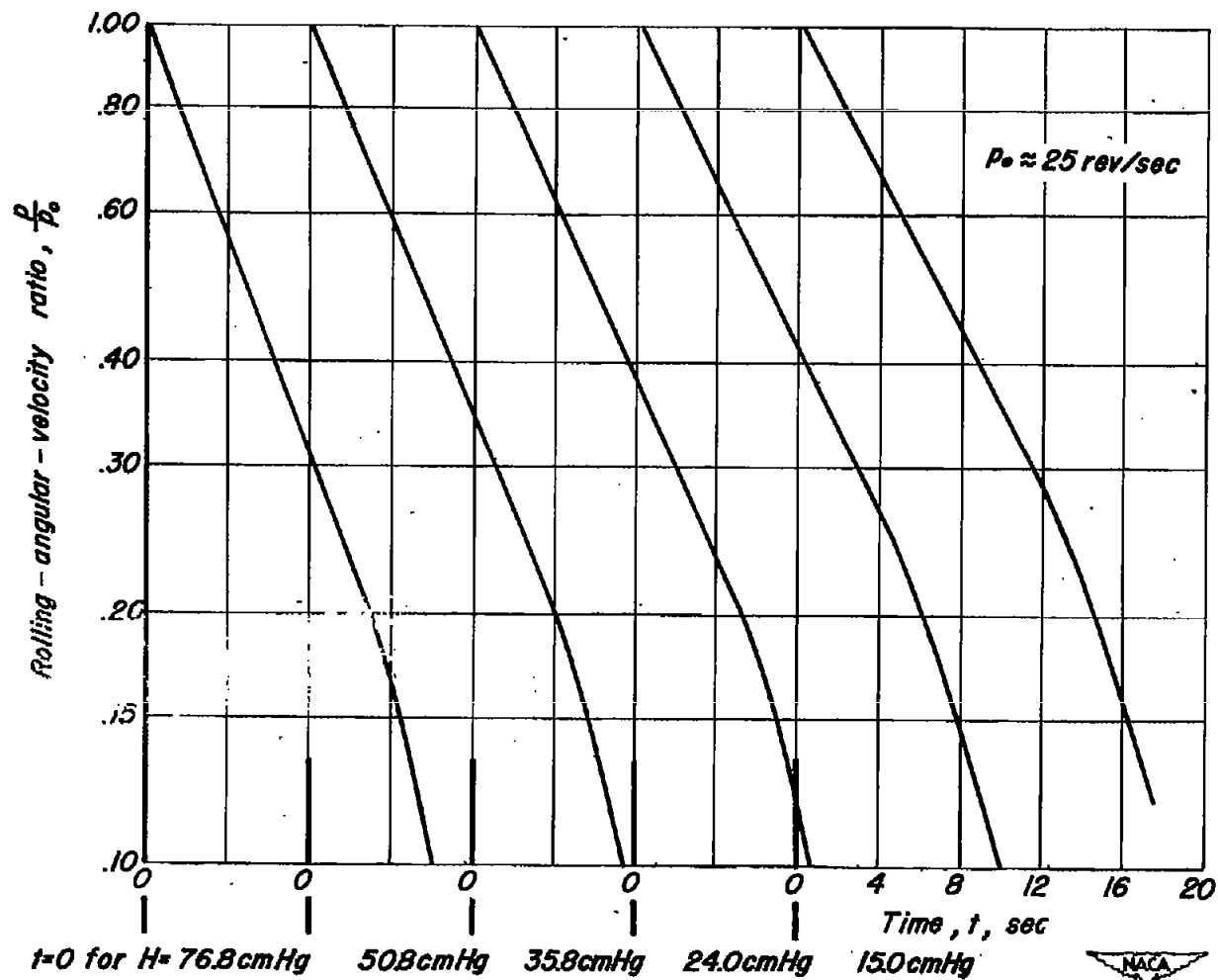
Figure 12. — Wind-off time histories of the rolling-angular-velocity ratio, $\frac{p}{p_o}$, for the slotted-fin configuration.

Figure 13. — Variation of the friction damping parameter, F_p/I_x, with tunnel total pressure, H, for the 8-cm aircraft rocket.
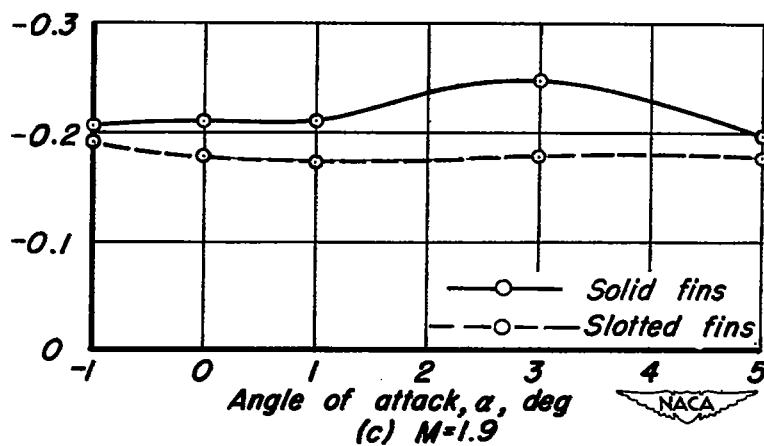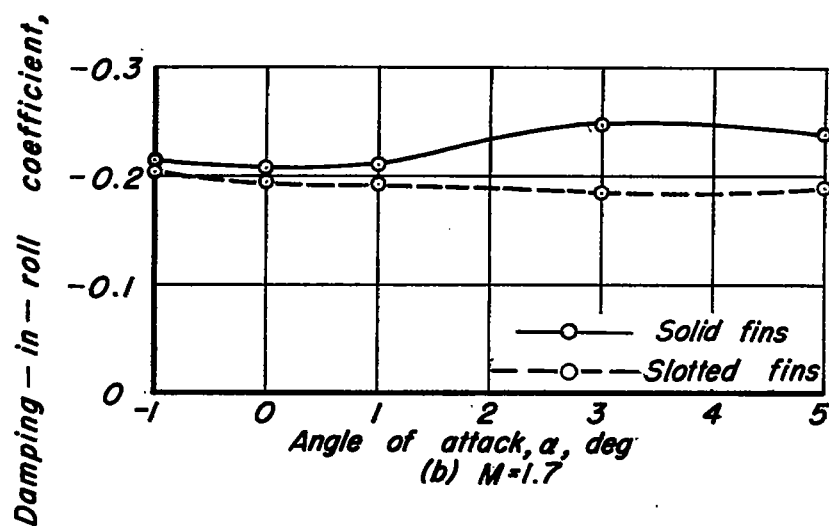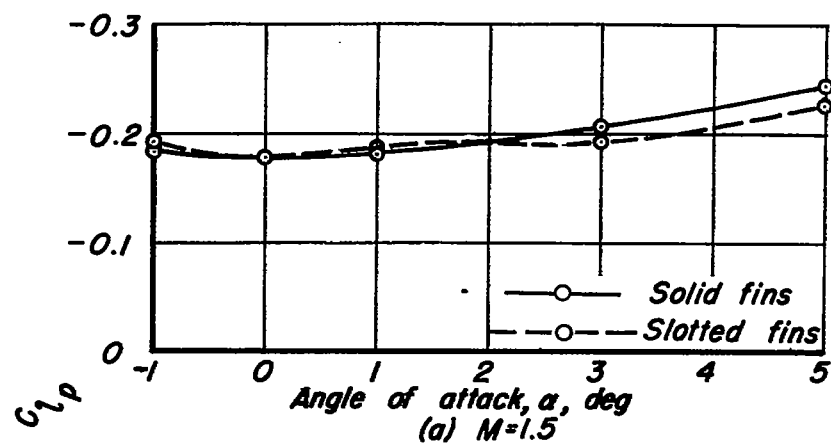
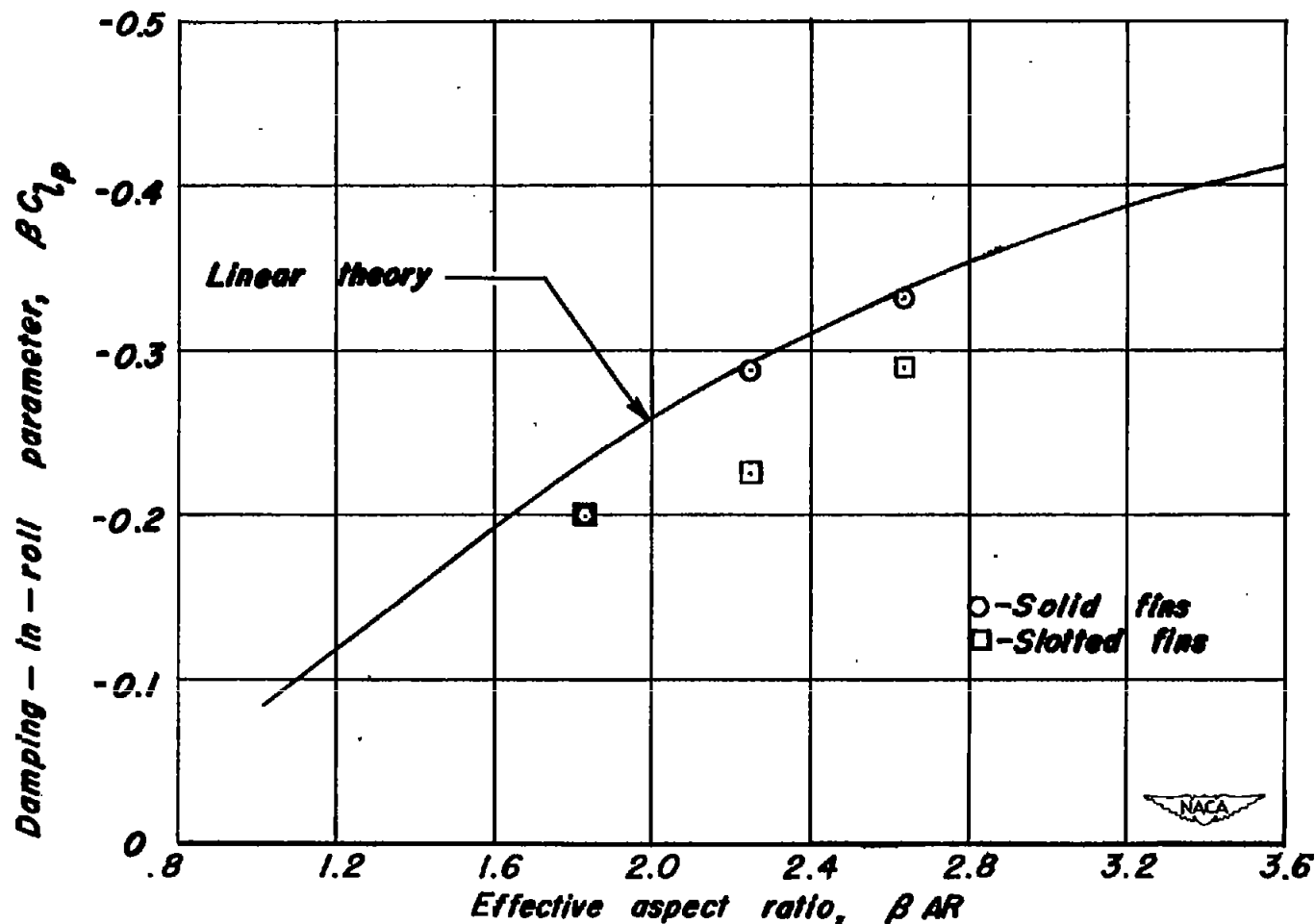Figure 14.—Variation of damping-in-roll coefficient with angle of attack for the 8-cm aircraft rocket.

Figure 15. - Variation of damping-in-roll parameter, βC_{l_p}, with effective aspect ratio, βAR, for the 8-cm aircraft rocket at $\alpha = 0°$.